



**NTNU – Trondheim**  
Norwegian University of  
Science and Technology

# Design of multiple air gap generator for renewable energy

**Rune Oterhals**  
**Torstein Ohr**

Product Design and Manufacturing  
Submission date: June 2012  
Supervisor: Terje Rølvåg, IPM

Norwegian University of Science and Technology  
Department of Engineering Design and Materials



THE NORWEGIAN UNIVERSITY  
OF SCIENCE AND TECHNOLOGY  
DEPARTMENT OF ENGINEERING DESIGN  
AND MATERIALS

**MASTER THESIS SPRING 2012  
FOR  
STUD. TECHN. TORSTEIN OHR OG  
STUD. TECHN. RUNE OTERHALS**

**DESIGN AV MULTIPPEL AIR GAP GENERATOR FOR FORNYBAR ENERGI**  
**Design of multiple air gap generator for renewable energy**

SmartMotor AS localized in Trondheim develops and produces electric generators using permanent magnets and are one of the leading companies within this field. SmartMotor is currently developing a new type of generator for use in tidal energy.

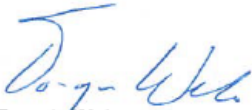
The work will include the following tasks:

1. Define a generator requirement specification
2. Carry out mechanical design of multiple air gap (M.A.G.) machine for direct-driven tidal turbine of 1.1 MW
3. Make assembly-friendly design (safe and cheap to put the machine together).
4. Optimize the machine with regards to (without compromising reliability):
  - a. minimum outer diameter
  - b. number of air gaps
  - c. configurations of active parts
  - d. use of lightweight materials (e.g. composites)

The thesis should include the signed problem text, and be written as a research report with summary both in English and Norwegian, conclusion, literature references, table of contents, etc. During preparation of the text, the candidate should make efforts to create a well arranged and well written report. To ease the evaluation of the thesis, it is important to cross-reference text, tables and figures. For evaluation of the work a thorough discussion of results is appreciated.

Three weeks after start of the thesis work, an A3 sheet illustrating the work is to be handed in. A template for this presentation is available on the IPM's web site under the menu "Undervisning". This sheet should be updated when the Master's thesis is submitted.

The thesis shall be submitted electronically via DAIM, NTNU's system for Digital Archiving and Submission of Master's thesis.



Torgeir Welo  
Head of Division



Terje Rølvåg  
Professor/Supervisor



NTNU  
Norges teknisk-  
naturvitenskapelige universitet

Institutt for produktutvikling  
og materialer

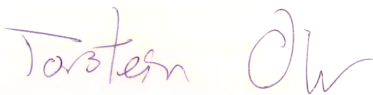
# Foreword

This thesis is written at NTNU and is a result of a cooperation with the Department of Engineering Design and Materials, and SmartMotor A/S. The report have been written as a collaboration between us two students.

SmartMotor was the first to propose the project task, as result of a new electromagnetic design idea. Our task were to develop a mechanical structure for a generator using the new electromagnetic design idea.

During the project period we have had regular contact with our supervisor Terje Rølvåg, professor at the Department of Engineering Design and Materials, and our contact persons at SmartMotor, Alexey Matveev and Rune Motoren Haug. We will thank our supervisor and SmartMotor for helpful guidance and assistance.

UGS NX 7.5 was used to perform the analysis. The project was written in L<sup>A</sup>T<sub>E</sub>X, a front end software for L<sup>A</sup>T<sub>E</sub>X.



Torstein Ohr



Rune Oterhals



# Contents

<b>Foreword</b>	<b>i</b>
<b>Summary</b>	<b>xiii</b>
<b>Summary - Norwegian</b>	<b>xv</b>
<b>1 Introduction</b>	<b>1</b>
<b>2 Theory</b>	<b>3</b>
2.1 Multiple air gap generator principle . . . . .	3
2.2 Electromagnetic theory . . . . .	6
2.3 Requirement specifications . . . . .	7
2.4 Load case . . . . .	8
2.4.1 Rotor - stator interaction . . . . .	9
2.4.2 Rotor, magnet - magnet interaction, only radial forces . . . . .	13
<b>3 Concept development</b>	<b>15</b>
3.1 Partial solutions . . . . .	16
3.1.1 Main structure of the stator . . . . .	16
3.1.2 Main structure of the rotor . . . . .	17
3.1.3 Carrying element for active parts of the rotor and stator . . . . .	17
3.1.4 Cooling of stator . . . . .	18
3.1.5 Morphology of partial solutions . . . . .	18
3.2 Evaluation of partial solutions . . . . .	20
3.2.1 Rotor main structure . . . . .	20
3.2.2 Stator main structure . . . . .	20
3.2.3 Fastening of rings . . . . .	21
3.2.4 Tracks for laminations . . . . .	22
3.2.5 Cooling of stator . . . . .	23
3.3 Chosen carrying structure solutions . . . . .	25
3.3.1 Assembly . . . . .	27
<b>4 Design and analysis</b>	<b>29</b>
4.1 Objective of task . . . . .	29
4.2 Summary . . . . .	30
4.2.1 Load cases . . . . .	30
4.2.2 Tools . . . . .	30

4.2.3	Materials . . . . .	30
4.2.4	Results . . . . .	31
4.3	Design . . . . .	32
4.3.1	Ring dimensions . . . . .	35
4.4	Rotor and stator structure material data . . . . .	37
4.4.1	Material properties . . . . .	37
4.4.2	Fatigue properties . . . . .	38
4.5	Safety factors . . . . .	39
4.5.1	ULS safety factor . . . . .	39
4.5.2	ULS safety factor - lifting . . . . .	39
4.5.3	FLS safety factors . . . . .	39
4.5.4	ELS safety factors . . . . .	40
4.6	Load cases . . . . .	42
4.6.1	Load cases for rings . . . . .	43
4.6.2	Rotor and stator structure assembly . . . . .	44
4.7	Simulation setup . . . . .	47
4.7.1	Rings simulation setup . . . . .	47
4.7.2	Rotor and stator structure simulation setup . . . . .	48
4.7.3	Lifting scenario simulation setup . . . . .	50
4.7.4	Rail simulation setup . . . . .	51
4.8	Summary of preliminary static and eigenmode simulations . . . . .	53
4.9	Final simulations . . . . .	54
4.9.1	FLS results . . . . .	54
4.9.2	ULS results . . . . .	63
4.9.3	ELS results . . . . .	67
4.10	Lightweight materials . . . . .	69
4.11	Assembly . . . . .	71
<b>5</b>	<b>Conclusion</b>	<b>77</b>
5.1	Results . . . . .	77
5.2	Discussion . . . . .	78
<b>6</b>	<b>Appendix A - Simulation ring vs beams</b>	<b>79</b>
<b>7</b>	<b>Appendix B - Preliminary simulations results</b>	<b>83</b>
7.1	Static ring simulations . . . . .	83
7.2	Static rotor structure simulations . . . . .	85
7.3	Static stator structure simulations . . . . .	87
7.4	Eigenmode simulations . . . . .	88
7.4.1	Rotor . . . . .	88
7.4.2	Stator . . . . .	89
<b>8</b>	<b>Appendix C - Material</b>	<b>91</b>
<b>9</b>	<b>Appendix D - Fatigue calculations</b>	<b>97</b>
9.1	Calculation of effective stress notch amplitude . . . . .	97



## Contents

---

9.2	Calculation of surface finish factor $f_s$ . . . . .	98
9.2.1	Calculation of wall thickness correction factor . . . . .	99
9.3	Calculation of temperature correction factor . . . . .	99
9.4	Calculation of mean stress correction factor . . . . .	99
9.5	Partial material factor . . . . .	99
9.6	Consequence of failure factor . . . . .	100
<b>10</b>	<b>Appendix E - Weight estimations of the final generator parts</b>	<b>101</b>
<b>11</b>	<b>Appendix F - Power output calculations</b>	<b>105</b>
	<b>Bibliography</b>	<b>107</b>



# List of Figures

2.1	Aerodynamics, small vs large generator diameter . . . . .	3
2.2	Radial and axial flux multiple air gap principle . . . . .	4
2.3	SmartMotor multi air gap generator principle sketch . . . . .	5
2.4	The laminated sheet metal which holds the magnets . . . . .	6
2.5	Flux path in the rotor (magnets and laminations) . . . . .	6
2.6	Force components acting on both the stator and rotor from the rotor-stator interaction . . . . .	8
2.7	Radial forces acting on the stator teeth at a given moment . . . . .	9
2.8	Radial forces generated from rotor-stator interaction, acting on 4 consecutive stator teeth. 5mm air gap, 11rpm, 2665.5mm air gap diameter, 132 magnets and 144 stator teeth . . . . .	9
2.9	Tangential forces generated from rotor-stator interaction, acting on 4 consecutive stator teeth. 5mm air gap, 11rpm, 2665.5mm air gap diameter, 132 magnets and 144 stator teeth . . . . .	10
2.10	Short circuit radial forces generated from rotor-stator interaction, every second consecutive stator tooth. 3mm air gap, 11rpm, 2665.5mm air gap diameter, 132 magnets and 144 stator teeth . . . . .	11
2.11	Radial forces acting on the stator from rotor-stator interaction with 5mm, 4mm and 3mm air gap. 11rpm, 2665.5mm air gap diameter, 132 magnets and 144 stator teeth . . . . .	13
3.1	Tree view of the generator parts . . . . .	15
3.2	Main parts of the generator carrying structure . . . . .	16
3.3	Insertion of magnets and laminations through the main structure of the stator . . . . .	17
3.4	Carrying elements for active parts, rings vs. beams . . . . .	18
3.5	Chosen solution rotor structure . . . . .	20
3.6	Chosen solution stator structure . . . . .	21
3.7	Track bolting to a ring . . . . .	22
3.8	Solution for the rail bolt connection . . . . .	23
3.9	Chosen stator cooling solution. Cooling tubes seen in the radial direction to the left and axial direction to the right . . . . .	24
3.10	Stator structure with rings . . . . .	25
3.11	Rotor structure with axle and rings . . . . .	25
3.12	Segment of laminations and magnets attached to the rotor . . . . .	26
3.13	Complete assembly of the generator with holes for insertion of magnet and lamination segments . . . . .	26

3.14	Assembly, step by step progress . . . . .	27
4.1	Final generator . . . . .	32
4.2	Sectioned view of the generator including axle and bearings . . . . .	32
4.3	Rotor structure including magnet and lamination sections (11 sections per ring side) . . . . .	33
4.4	Sectioned view of the rotor structure . . . . .	33
4.5	Sectioned view of the stator including active parts and cooling tubes . . . . .	34
4.6	Sectioned view of the stator structure . . . . .	34
4.7	Magnets and lamination sections for outer and inner rotor ring. 12 magnets per sections. 3 rails per section for outer rings and 2 rails for inner rings . . . . .	35
4.8	Ring, flange and active parts dimensions . . . . .	36
4.9	Outer stator ring flange dimensions . . . . .	37
4.10	Worst case load, rotor main structure . . . . .	44
4.11	Worst case loads, stator main structure . . . . .	45
4.12	Fixed constraint and forces on the stator ring simulation model . . . . .	48
4.13	Simulation model rotor main structure . . . . .	49
4.14	Stator simulation setup - forces applied to inner and middle stator rings . . . . .	50
4.15	Stator simulation setup - fixed constrain on torque plate . . . . .	50
4.16	Lifting simulation setup . . . . .	51
4.17	Mesh, constraints and forces in rail simulation . . . . .	52
4.18	Shape and dimensions of the rail . . . . .	52
4.19	Inner rotor ring elemental stresses, final simulation . . . . .	54
4.20	Inner rotor ring displacement, final simulation . . . . .	55
4.21	Outer rotor ring elemental stresses, final simulation . . . . .	56
4.22	Outer rotor ring displacement, final simulation . . . . .	56
4.23	Inner stator ring elemental stresses, final simulation LC2 . . . . .	57
4.24	Inner stator ring displacement, final simulation LC2 . . . . .	58
4.25	Middle stator ring elemental stresses, final simulation . . . . .	59
4.26	Middle stator ring displacement, final simulation . . . . .	59
4.27	Outer stator ring elemental stresses, final simulation LC2 . . . . .	60
4.28	Outer stator ring displacement, final simulation LC2 . . . . .	61
4.29	Deformations on the rail with SSL=730mm . . . . .	62
4.30	Elemental stresses on the rail with SSL=730mm . . . . .	62
4.31	Rotor structure displacement . . . . .	63
4.32	Rotor structure elemental stresses . . . . .	64
4.33	Stator structure displacement . . . . .	65
4.34	Stator structure elemental stresses . . . . .	65
4.35	Displacement from the lifting simulation . . . . .	66
4.36	Stresses from the lifting simulation . . . . .	67
4.37	Rotor structure eigenmode simulation final result. Deformation values does not represent real deformations . . . . .	68
4.38	Stator structure eigenmode simulation final result. Deformation values does not represent real deformations . . . . .	69

4.39	Welding of stopping plates . . . . .	71
4.40	Mounting of stiffening parts to the rotor torque plate . . . . .	71
4.41	Bolting of rails to ring . . . . .	72
4.42	Laminations shrunk onto the middle stator ring . . . . .	72
4.43	Bolting of stator rings to torque plate . . . . .	73
4.44	Mounting torque plate and outer stator ring together . . . . .	73
4.45	Rotor torque plate, rings and axle assembly . . . . .	74
4.46	Stator and rotor structure assembled . . . . .	74
4.47	Rotor torque plate and rings are slid into the stator . . . . .	75
4.48	Insertion of magnet segments . . . . .	75
6.1	Simulation setup of the ring . . . . .	79
6.2	Simulation setup of the beams . . . . .	80
6.3	Ring with axial length of 1000mm, displacements . . . . .	81
6.4	Radial displacement, ring with 400mm axial length . . . . .	81
6.5	Radial displacement, segment of beams connected with a thin ring. Axial beam length of 400mm . . . . .	82
7.1	Rotor ring deformations. 22 rails, axial length 700mm and diameter of 1810 mm . . . . .	84
7.2	Stator middle ring deformations, axial length 700mm and diameter of 1419mm . . . . .	85
7.3	Rotor deformations, simplified simulations . . . . .	86
7.4	Magnitude of deformations for rotor, SSL=0,6m . . . . .	86
7.5	Stator deformations, simplified simulations . . . . .	87
7.6	Magnitude of deformations for stator, SSL=0,6m . . . . .	88
7.7	Stiffening plates and ring, rotor structure . . . . .	89
7.8	Deformations from eigenmode simulations on the stator . . . . .	90
10.1	Weight calculations from electromagnetic simulations at SmartMotor . .	102
11.1	Power output calculations. Screenshot from Excel . . . . .	105



# List of Tables

2.1	Requirement specifications . . . . .	7
3.1	Morphology table . . . . .	19
3.2	Evaluation of track-alternatives for a rotor/stator ring . . . . .	23
4.1	Load cases used for each part . . . . .	30
4.2	Suggested material for the parts of the carrying structure . . . . .	30
4.3	Final simulations of the rings and rail, FLS results . . . . .	31
4.4	Final simulations of the rotor and stator assembly, ULS and ELS results	31
4.5	Ring dimensions and weight. There are two of each ring except the outer stator ring . . . . .	35
4.6	Ring dimensions . . . . .	36
4.7	Material data for rotor and stator structure . . . . .	37
4.8	Lamination material properties in NX . . . . .	38
4.9	Fatigue properties from CES EduPack . . . . .	38
4.10	FLS safety factors . . . . .	39
4.11	Surface finish factor . . . . .	40
4.12	Frequency and phase difference . . . . .	42
4.13	Normal operation force parameters, 3mm air gap. Force values are for each tooth/magnet per meter in the axial direction . . . . .	42
4.14	Radial forces. Short circuit force parameters, 3mm air gap. Force values are for each tooth/magnet per meter in the axial direction . . . . .	42
4.15	Tangential forces. Normal operation parameters. Force values are for each tooth/magnet per meter in the axial direction . . . . .	43
4.16	Forces on each rail . . . . .	44
4.17	Rotor structure forces . . . . .	45
4.18	Final results of inner rotor ring, LC1 . . . . .	54
4.19	Final results of outer rotor ring . . . . .	55
4.20	Final results of inner stator ring . . . . .	57
4.21	Final results of middle stator ring . . . . .	58
4.22	Final results of outer stator ring . . . . .	60
4.23	Final simulation result of the rail, LC5 . . . . .	61
4.24	Final results rotor structure assembly . . . . .	63
4.25	Final results stator structure assembly . . . . .	64
4.26	Results, lifting scenario . . . . .	66
4.27	Final results rotor structure, eigenmode simulation . . . . .	67
4.28	Final results stator structure, eigenmode simulation . . . . .	68

---

4.29	Result from the eigenmode simulations of the stator structure in aluminum and steel . . . . .	70
6.1	Results from the simulations on rings, with radial and tangential forces	80
6.2	Results from the simulations on beams, with radial and tangential forces	80
7.1	Results from the preliminary rotor ring simulations . . . . .	83
7.2	Results from the preliminary stator ring simulations . . . . .	84
9.1	Surface finish factor . . . . .	98
10.1	Weight estimates for the generator parts . . . . .	103



# Summary

The purpose of this project was to design and analyze the carrying structure of a multiple air gap generator for tidal turbine application. An initial patent pending electromagnetic design was provided by SmartMotor AS. Electromagnetic values, such as forces from the rotor-stator interaction, were given by SmartMotor. The final product is a 3D-model of the generator with dimensions and shape based on required power output, production and assembly limitations and static and eigenmode simulations.

The multiple air gap principle allows for a more compact generator, as there are several layers - in the radial direction - of rotors (magnets) and stators (windings) instead of one set of rotor and stator. A generator normally uses a gearbox to increase power output. This however increases maintenance and introduces more friction losses. By using multiple air gaps, the generator can potentially maintain the same size and power output while eliminating the gearbox.

The multiple air gap principle, as well as some basic electromagnetic theory, was discussed to give an insight in the planned generator. A requirement specification was set, with the most important ones being a power output of 1.1 MW and a maximum outer diameter of 3m. The rotor has 132 magnets in each layer and the stator 144 teeth, creating a varying force between the rotor and the stator. The air gap in each layer is initially 5mm, and the forces increase if the air gap gets smaller.

To evaluate different solutions for the carrying structure, the generator was broken down into smaller parts. Several design ideas were evaluated and discussed with engineers at SmartMotor. The chosen design was influenced especially by deformation and production/cost demands. Complex shapes become expensive and difficult to produce when the total diameter is above two meters. Instead it is used torque plates to counteract the torque forces and radial plates to counteract the bending from the radial forces. The most challenging parts to produce are the rings, which both the stator and rotor active parts are mounted to. These have to be casted due to its large size.

The chosen design was modeled and analyzed for deformations and stresses in UGS NX 7.5. To reduce simulation time and the complexity of the model, the stator, rotor and rings were simulated separately. Some simplifications and assumptions had to be done, but always on the conservative side. The results from the static simulations showed that increasing the axial length and decreasing the diameter resulted in a stiffer structure. The rotor and stator structure were also analyzed for eigenfrequencies in UGS NX, and it was these simulations which set the final dimensions for the generator structure.

The final generator has an outer diameter of 2.32m, a total length of 2.035m (excluding bearings) and uses 4 air gap layers. The total weight was estimated to 25.4 tons. A step-by-step description of the generator assembly was presented. Finally possible sources of error in the simulations and further work on the generator were discussed.

# Summary - Norwegian

Formålet med dette prosjektet var å konstruere og analysere den bærende strukturen for en multippel luftgaps-generator for bruk i en tidevannsturbin. Et initielt patentanmeldt design var gitt av SmartMotor AS. Elektromagnetiske parametere var gitt av SmartMotor, inkludert kreftene mellom rotor og stator. The endelige produkt er en 3D-modell av generatoren, der de endelige dimensjonene er basert på simuleringer og krav til effekt, produksjon og sammensetning.

Vanligvis brukes en girboks i kombinasjon med generatoren for å øke effekten. En girboks gir derimot større friksjonstap og mer vedlikehold. Ved å bruke flere lag med magneter (rotor) og vindinger (stator) kan generatoren potensielt lages like kompakt som en én-lagsgenerator (medregnet girboks), samtidig som girboksen droppes.

For å få innsikt i den planlagte generatoren ble prinsippet om multippel luftgap og grunnleggende elektromagnetisk teori diskutert. En kravspesifikasjon ble satt; hvor et effektkrav på 1,1 MW og en maksimum ytre diameter på 3m var de viktigste kravene. Rotoren har 132 magneter i hvert lag, og statoren 144 tenner, som gir varierende krefter mellom rotor og stator. Luftgapet er satt til 5mm, men et mindre luftgap pga deformasjoner og skjev montering/produksjon vil gi økte krefter.

For å vurdere forskjellige løsninger for den bærende strukturen ble generatoren delt opp i mindre deler. Flere design-idéer ble vurdert i samarbeid med ingeniører hos SmartMotor. Det valgte designet er hovedsakelig basert på krav til stivhet, produksjon og kostnader. Komplekse former blir utfordrende og kostbare å produsere ved en totaltdiameter over 2m. Derfor er det brukt torque-plater for å motvirke dreiemoment og radielle plater for å motvirke bøyning fra kreftene mellom rotor og stator. De mest utfordrende delene å produsere er ringene grunnet deres store størrelse. Disse må støpes og deretter maskineres.

Det valgte designet var modellert og analysert for deformasjoner og spenninger i UGS NX 7.5. For å redusere simuleringstiden og kompleksiteten av modellen ble rotor, stator og ringene simulert hver for seg. Noen forenklinger og antagelser var gjort, men alltid på den konservative siden. Resultatene fra simuleringene viste at økt aksial lengde og redusert diameter ga en stivere struktur. Både rotor og stator var også analysert for egenfrekvenser i UGS NX, og det var disse simuleringene som ble dimensjonerende for generatorstrukturen.

Den endelige generatoren har 4 luftgap, en ytterdiameter på 2.32m og en total lengde på 2.035m (ekskludert lager). Totalvekten ble estimert til 25.4 tonn. En punktvis beskrivelse av sammensetningen av generatoren ble presentert. Til slutt ble mulige feilkilder i simuleringene og videre arbeid med generatoren diskutert.



# 1 Introduction

SmartMotor A/S [1] is a firm located in Trondheim which has specialized on designing electric motors and generators. SmartMotor is one of the leading companies on electromagnetic parts in motors and generators. They have a patent pending on a new and advantageous electromagnetic design for a generator.

The electromagnetic design uses the multiple air gap principle, and the air gaps are placed in layers with different diameters. In theory a generator using this new principle can with the same diameter, generate the required power without the use of a gearbox. This is also the main motivation behind the project, as it is preferable to have a small generator diameter, and not use a gearbox in tidal turbines and windmill applications. A gearbox increases total friction losses and the need for maintenance. A large generator diameter also reduces the flow around the turbine.

The goal of this report is to go from the electromagnetic design idea, to a mechanical carrying structure for such generator. The whole design process will be illustrated, starting with background theory to acquire the needed understanding and to illustrate the function and advantages of the electromagnetic design idea. Then follows the development and selection of partial solutions for the different functions and parts. The last sections include the actual modeling and analysis, including description of the simulation setup and evaluation of the results.

From a mechanical point of view this new principle creates challenges, as there are generated large forces in each air gap. The carrying structure of the generator must support the active parts of every air gap. It was challenging to achieve the desired stiffness of the structure, as there is limited space around the active parts. The main focus of the project has been the main parts of the carrying structure of the generator; smaller details such as bolt connections, selection of exact bearing and axle design have been left out. Due to a complex load cases, simplifications have been done in the setup of the simulations, especially during the simulations of the main structures of the rotor and stator. All simplifications have been conservative, giving the structure an additional safety factor.

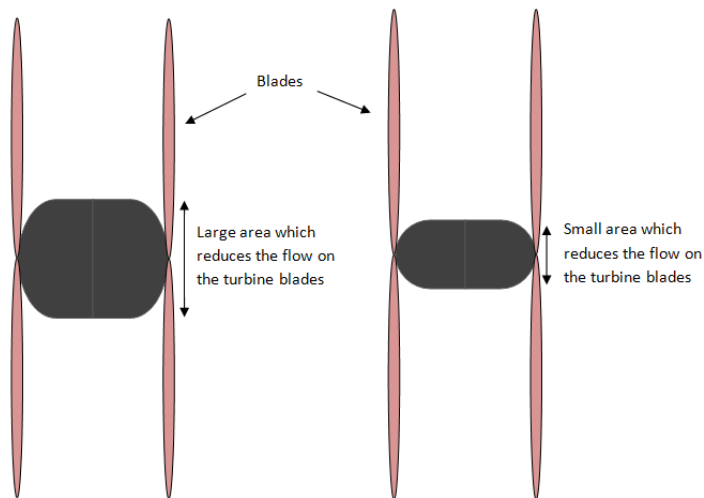


## 2 Theory

### 2.1 Multiple air gap generator principle

Power output, size and weight are important parameters when comparing different generators. As generator output power is the product of torque and speed between the rotor and stator, we get the following relationship: higher speed means lower torque for a given power, and a more compact generator can be achieved. The generator must either (or both) have a large diameter or be connected to a gearbox which increases the rotor speed.

In a tidal turbine application, a large generator diameter gives reduced aerodynamic properties due to the water flow around the generator (Figure 2.1). In addition, transportation of the generator on land becomes an issue if the diameter is larger than 4m.

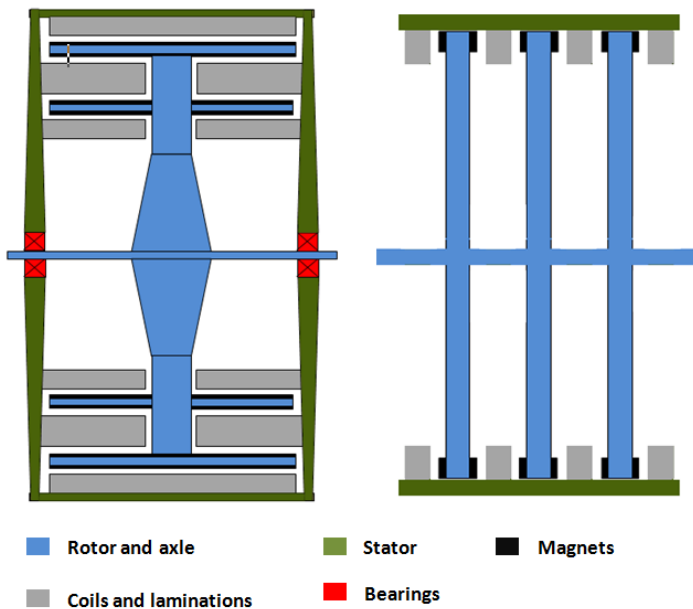


**Figure 2.1:** Aerodynamics, small vs large generator diameter

Gearboxes are used to speed up the generator, so the diameter can be reduced and still have the same power output. However, using a gearbox has some disadvantages:

- Friction losses
- More maintenance
- Less reliability

The multiple air gap principle makes it possible to keep the diameter fairly small without a gearbox. By having several air gap layers, either in the axial or radial direction (Figure 2.2), the power output will increase compared to a single layer generator of the same diameter. The number of layers are only limited by the maximum outer dimensions and the weight.



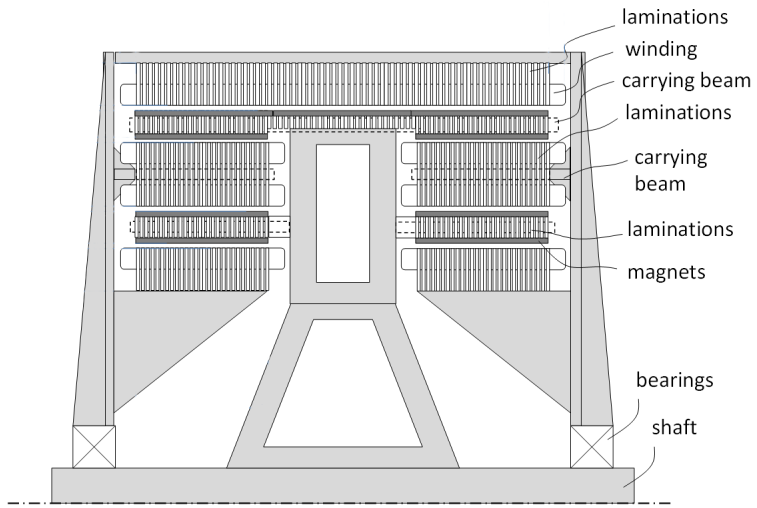
**Figure 2.2:** Radial and axial flux multiple air gap principle

SmartMotor wants to develop a multi air gap generator which uses the radial-flux principle. Their initial principle sketch of the generator is shown in Figure 2.3, which is patent pending. The turbine blades are connected to the center shaft, where the rotor is attached. Axially aligned beams are in turn connected to the rotor, holding laminations and permanent magnets. Beams are also connected to the stator housing, but these hold laminations and windings in place. A small air gap is necessary to minimize the use of permanent magnet material, and an air gap of maximum 5mm is desired from SmartMotor. The generator uses 4 air gap layers, but this can be altered as necessary. However, having air gaps close to the center shaft will not produce much torque and power, as the relative speed between the rotor and stator will be low.



## 2.1 Multiple air gap generator principle

---

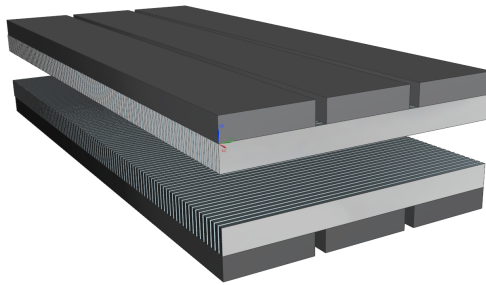


**Figure 2.3:** SmartMotor multi air gap generator principle sketch

## 2.2 Electromagnetic theory

The generator principle in this case uses permanent magnets. Power is produced when the magnetic field around a conductor changes. The magnets are attached to a rotor, every other with a north and south side facing the windings in the stator. As the magnets pass by the static windings, the magnet field changes.

The magnets are held in place by using laminated sheet metal between the magnets and the carrying structure (Figure 2.4). The laminations are stacked axially to avoid circulating currents, only allowing the flux to move the shortest distance possible between magnets (Figure 2.5). The permanent magnets are blocks made of an iron alloy.

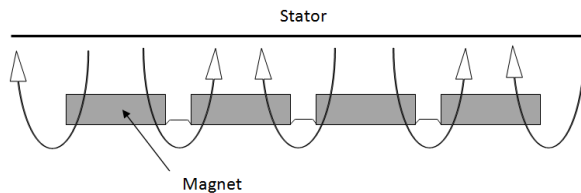


**Figure 2.4:** The laminated sheet metal which holds the magnets

The frequency of the generator is determined by how often the magnetic field changes, a faster field change gives a higher power output. This means that it is beneficial to have as many magnetic poles as possible to get a high frequency. Large magnets are also beneficial as increased magnet size gives a stronger magnetic field, but this reduces the frequency due to space limitations.

The air gap between the magnets and the stator windings also influences the amount of power that is generated. A smaller air gap reduces the resistance for the flux as it is moving between the magnets and the stator windings. This results in a higher power output.

The support structure for the magnets, laminations and the windings has to be non-magnetic or insulated as to avoid circulating currents.



**Figure 2.5:** Flux path in the rotor (magnets and laminations)

## 2.3 Requirement specifications

The generator is intended for use in a tidal turbine application, possibly replacing existing generators (which uses a gearbox). A specific application is the Atlantis Tidal Turbine [2], where SmartMotor already supplies the generators. The requirements for the new multiple air gap generator, given by SmartMotor, are presented in Table 2.1.

Property	Value/description
Power	1,1 MW
Max outer diameter	3 m
Desired outer diameter	2 m
Cooling	Oil, water for stator coils
Medium inside generator	Oil filled
Air gap	5mm
Propulsion	Center axle
Rotor magnets	Divided in segments, and inserted after the stator during assembly
Connection to turbine body	Bolting along stator edges

**Table 2.1:** Requirement specifications

The existing generator in the Atlantis Turbine has a diameter of about 2m. A direct-driven multiple air gap generator with the same diameter would be desired, but this may not be possible due to space limitations and structural difficulties. A maximum diameter of 3m would still be usable, as the improvements in maintenance, reliability and efficiency compensates for the increased diameter. There are however no limitations to the length of the generator.

The generator will produce heat which has to be removed. It is especially critical to cool down the stator windings, as they are the main heat source. It is sufficient to cool down the rotor magnets and laminations with oil. The parts in the generator are densely packed, which complicates the water cooling of the stator.

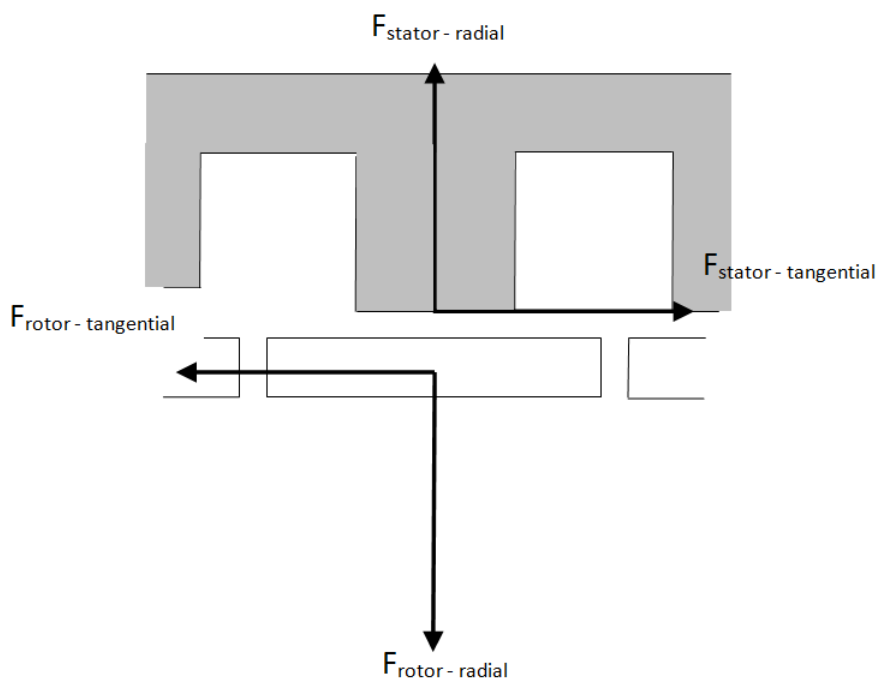
Weight is not an important factor for this generator, as the forces on the support structure for a tidal turbine are smaller in water than in air. However, a similar generator can also be used in a windmill application. A windmill has typically a taller structure because it needs larger turbine blades. In order to not make the windmill topheavy, the weight of the generator will be a more critical factor. In addition, the installation and lifting of the generator is easier if the weight is lower.

Electromagnetically, an air gap of 5mm is the desired maximum. This can of course be lower, resulting in higher power output, but structural difficulties may limit this. The accuracy of production and assembly may influence the necessary air gap size. In addition the parts will deflect because of varying forces.

## 2.4 Load case

When running the generator, the carrying structure will be exposed to constant static forces and oscillating forces which are dependent of the rotational speed. Both the rotor and the stator carrying structure must be designed with proper dimensions with respect to both static and dynamic load cases. For further explaining of the loads, the total load case will be divided in the following manner (Figure 2.6):

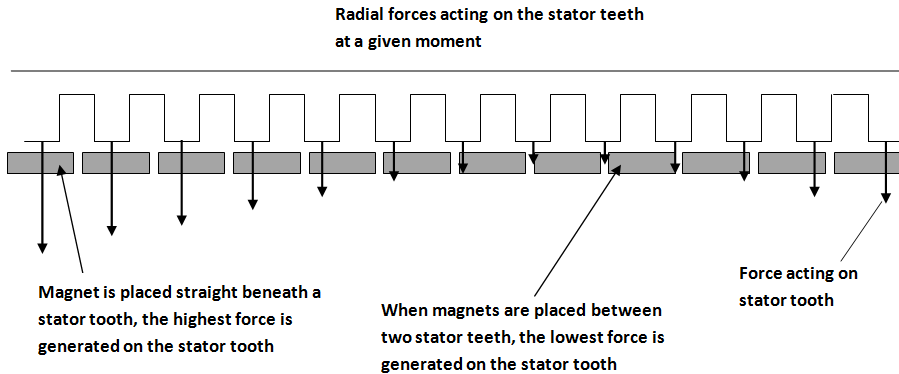
- Rotor - stator interaction
  - Oscillating radial forces
  - Oscillating tangential forces (torque-producing)
- Magnet - magnet interaction, static forces
  - Static attraction or repulsive forces



**Figure 2.6:** Force components acting on both the stator and rotor from the rotor-stator interaction

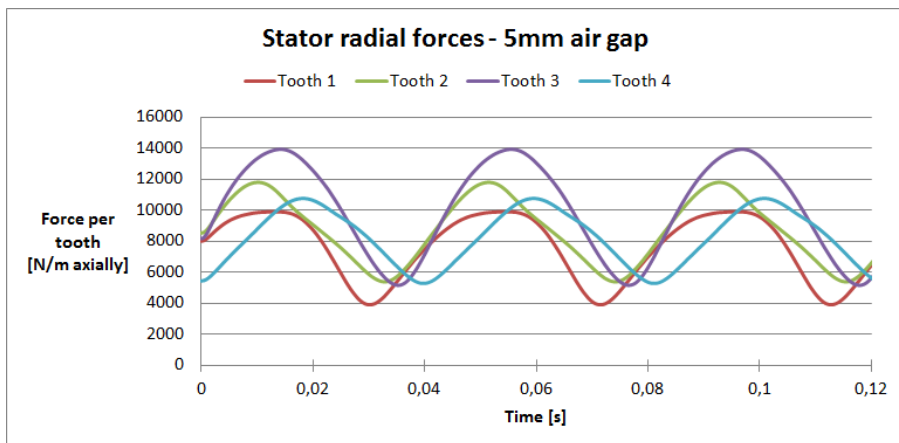
### 2.4.1 Rotor - stator interaction

As the magnets on the rotor are passing the stator windings, both radial forces and tangential forces (torque) are created (Figure 2.7). These forces are oscillating and the frequency of the forces are speed dependent.

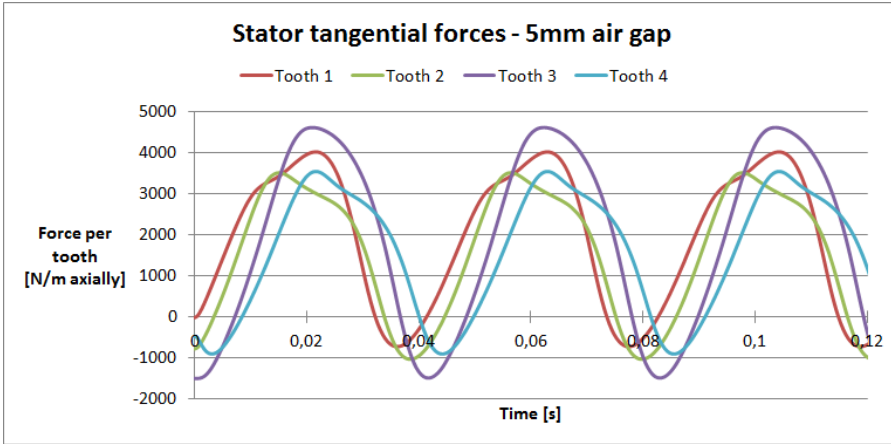


**Figure 2.7:** Radial forces acting on the stator teeth at a given moment

Each air gap is in force equilibrium, which means that the total forces acting on the magnets and the stator teeth sharing the same air gap is equal. The frequency of the forces changes proportionally with the rotational speed, and the carrying structure must withstand the forces at all speeds during operation.



**Figure 2.8:** Radial forces generated from rotor-stator interaction, acting on 4 consecutive stator teeth. 5mm air gap, 11rpm, 2665.5mm air gap diameter, 132 magnets and 144 stator teeth



**Figure 2.9:** Tangential forces generated from rotor-stator interaction, acting on 4 consecutive stator teeth. 5mm air gap, 11rpm, 2665.5mm air gap diameter, 132 magnets and 144 stator teeth

Due to the way the stator is electronically controlled, the amplitude of the forces will not be the same for each following magnet and stator tooth (Figure 2.8) (Figure 2.9). Every fourth tooth have the same amplitude and centerline value. This means that the force curve of tooth 5 will have the same amplitude and centerline value as the curve of tooth 1. If the stator short circuits different loads are generated. These forces are also oscillating, but with slightly different values (Figure 2.10). In the short circuit case every second force have the same amplitude and centerline value.

Neither the radial or the tangential forces are perfect sinusoidal curves. However, a sinusoidal curve would be a good approximation to the real force curves and will be used to approximate both the radial and the tangential oscillating loads:

$$F = A \sin(\omega t + \varphi) + B \quad (2.1)$$

$A$  =Amplitude [N]

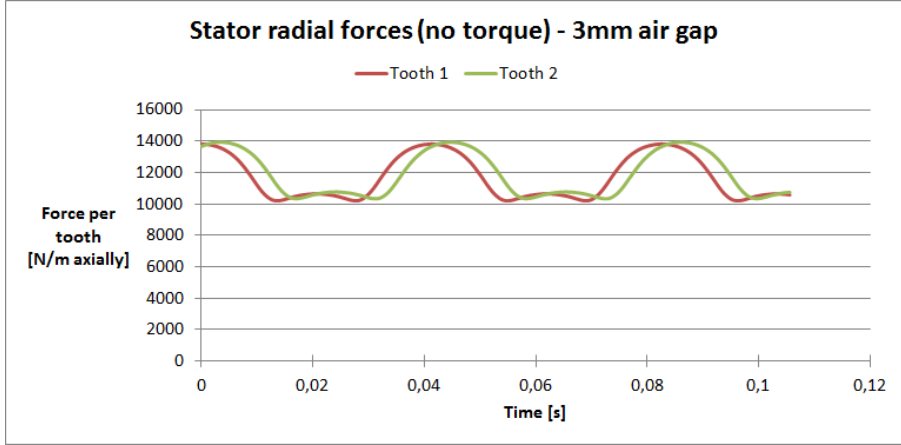
$\omega$  =Angular frequency of the sine curve [radians]

$t$  =time [s]

$B$  = Center line value [N]

$\varphi$  =Phase [radians]

The force frequency is as mentioned dependent of the generator speed, but the number of magnets and teeth on the stator are also important parameters. The reason for this



**Figure 2.10:** Short circuit radial forces generated from rotor-stator interaction, every second consecutive stator tooth. 3mm air gap, 11rpm, 2665.5mm air gap diameter, 132 magnets and 144 stator teeth

is that the frequency of the force acting on one specific stator tooth is determined by how often the magnets are passing this tooth (Equation 2.3). If the number of magnets were increased, magnets would pass this tooth more often at a given speed. The same applies for the force acting on one specific magnet (Equation 2.2), just in the opposite manner (dependent on the number of stator teeth). The frequency of the forces will be determined by the angular frequency of the sinus curves:

$$\omega_{rotor} = x_t \cdot 2\pi \cdot \frac{v}{60} \quad (2.2)$$

$$\omega_{stator} = x_m \cdot 2\pi \cdot \frac{v}{60} \quad (2.3)$$

$\omega_{rotor}$  = Angular frequency of the sine curve for the forces acting on the rotor [radians]

$\omega_{stator}$  = Angular frequency of the sine curve for the forces acting on the stator [radians]

$x_t$  = Number of stator teeth on each stator layer

$x_m$  = Number of magnets on each rotor layer

$v$  = Rotational speed [rpm]

If the number of stator teeth and rotor magnets are the same for each air gap, all forces acting on both the magnets and the stator teeth will be in phase. This is not relevant

for this generator due to cogging. A difference in magnets and stator teeth gives a phase difference between each magnet and stator force. The phase difference (Equation 2.4 and Equation 2.5) is proportional with the difference between the number of stator teeth and magnets sharing the same air gap:

$$\Delta\varphi_m = \frac{2\pi}{\left(\frac{x_m}{x_m - x_t}\right)} = \frac{(x_m - x_t) \cdot 2\pi}{x_m} \quad (2.4)$$

$$\Delta\varphi_t = \frac{2\pi}{\left(\frac{x_t}{x_m - x_t}\right)} = \frac{(x_t - x_m) \cdot 2\pi}{x_t} \quad (2.5)$$

$\Delta\varphi_m$  =Phase difference between each magnet [radians]

$\Delta\varphi_t$  = Phase difference between each stator tooth [radians]

Each following magnet of stator tooth adds a phase difference ( $\Delta\varphi$ ) to Equation 2.1:

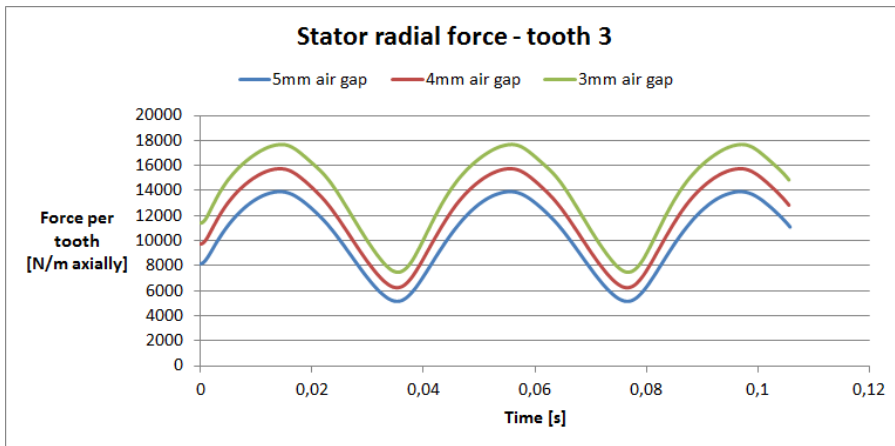
$$F_n = A \sin(\omega t + n \cdot \Delta\varphi) + B \quad (2.6)$$

$n$  =Magnet or stator tooth number

The frequency of the oscillating forces are dependent of the generator speed. These forces may induce vibrations to the structure. The resonance frequency of the carrying structure must, in relation to the frequency of the oscillating forces be analyzed.

If the deflections are large when the generator is running, the air gap distance might be altered. A smaller air gap gives higher forces, while a larger air gap gives smaller forces (Figure 2.11). This must be taken into account when dimensioning the carrying structure. From (Figure 2.11) shows that there is a linear coherence between the air gap and the magnitude of the forces between stator and rotor.





**Figure 2.11:** Radial forces acting on the stator from rotor-stator interaction with 5mm, 4mm and 3mm air gap. 11rpm, 2665.5mm air gap diameter, 132 magnets and 144 stator teeth

### 2.4.2 Rotor, magnet - magnet interaction, only radial forces

The forces between the magnets will be constant and not dependent on the rotational speed of the generator. However, SmartMotor has determined that these forces are so minor compared to the oscillating forces that they are insignificant.



### 3 Concept development

To evaluate and choose between different solutions for the carrying structure, the generator was broken down into smaller parts. Then partial solutions were defined and put together to a total result. Manufacturing, weight, costs, size, alignment accuracy, stiffness and assembly were important parameters when choosing the base structure design. The generator was first broken down into the following parts:

- Rotor
- Stator
- Axle

The carrying structure of both the stator and rotor are divided into two parts: One main part which is connected at the center and another part which is holding the active parts. The active parts will be designed by SmartMotor, except from the interface design between laminations and the carrying structure. The division of the generator parts is shown below:

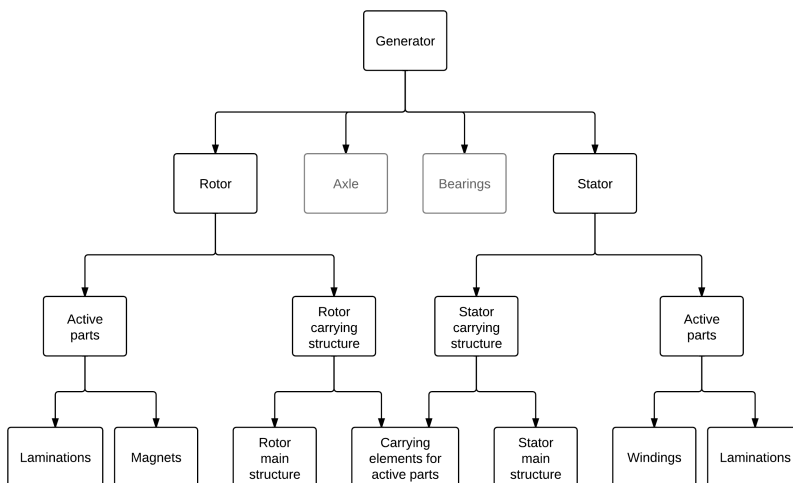
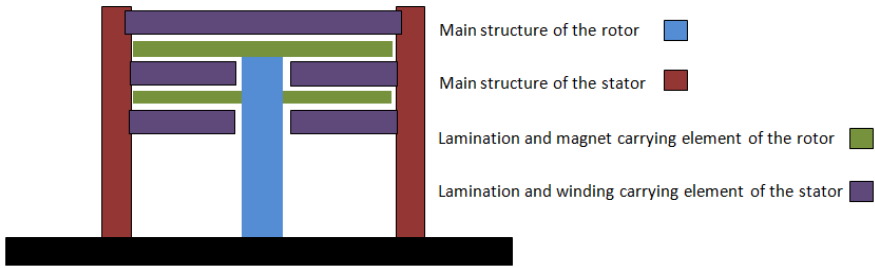


Figure 3.1: Tree view of the generator parts



**Figure 3.2:** Main parts of the generator carrying structure

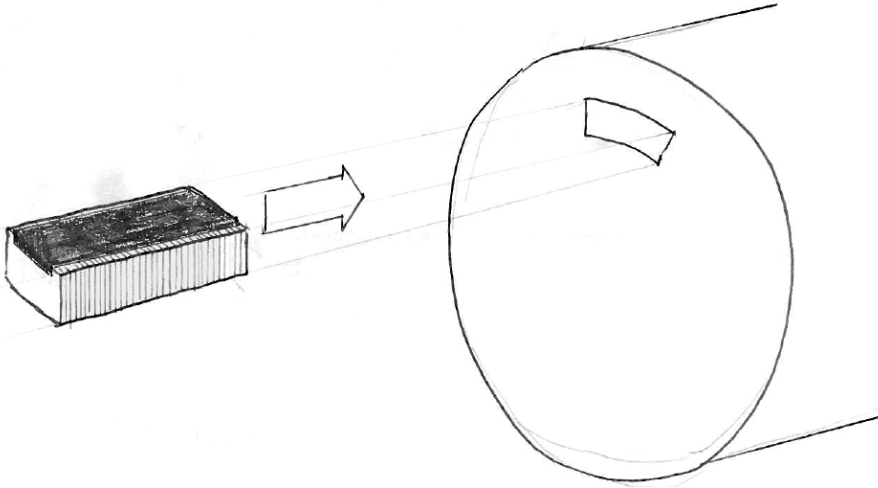
## 3.1 Partial solutions

Important parameters and requirements for each part of the carrying structure from Figure 3.2 will in this section first be discussed. Several partial solutions for each part were defined and evaluated. All solutions for the carrying structure are listed in Table 3.1. The best solution for each part was selected for further work in section 3.2.

### 3.1.1 Main structure of the stator

The stator will consist of two similar but mirrored outer main structural parts (Figure 3.2). The stator will not rotate during operation, and is connected to the bearing housing. The main stator structure must act as a rigid anchor point for the elements which holds the active parts of the stator. Due to vibrations and small tolerances, the stiffness of the main structure will probably be the dimensioning parameter.

One of the requirements of the generator is that it must be possible to insert the rotor magnets in smaller sections after the stator is mounted. If the stator is going to be connected to the rotor with all magnets inserted there will be very small tolerances for misalignment, and higher possibility for failure. This means that the sections/segments with magnets and laminations must be sled in place through the stator and onto the rotor. The stator must have openings which are big enough for one magnet/lamination section to go through, and onto the rotor (Figure 3.3).



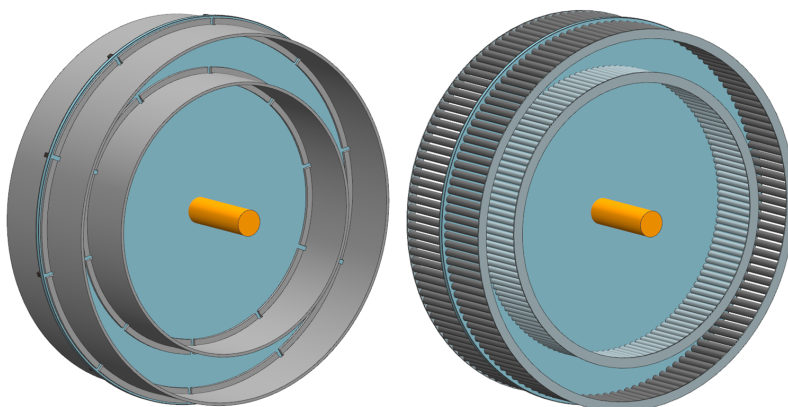
**Figure 3.3:** Insertion of magnets and laminations through the main structure of the stator

### 3.1.2 Main structure of the rotor

The rotor base structure is directly connected to the axle, and has to support the rotor active parts and withstand radial and tangential forces. Stiffness is, as for the stator, an important factor when designing the main structure.

### 3.1.3 Carrying element for active parts of the rotor and stator

The active parts must be held in place in radial layers of magnets and windings. Due to a small air gap and vibrations, only small displacements of these parts are allowed. In general there are two different ways of designing carrying elements for the active parts: either use a whole ring or numerous beams. Figure 3.4 shows how a setup of rings or beams would look like on the rotor. As the forces are the same on the stator active parts as on the rotor parts, the same design for the carrying elements can be used on both the stator and the rotor. Static simulations were performed to evaluate the stiffness of the two principles, and a ring proved to be 10 times stiffer than the beams at 400mm axial length. Setup, result and evaluations of these simulations are shown in Appendix A - Table 6.1 and Table 6.2.



**Figure 3.4:** Carrying elements for active parts, rings vs. beams

Using beams will require about one beam for each magnet, which results in approximately 500 beams for the complete rotor including both layers. The stator will also require about the same number of beams. Such high number of parts results in more work during assembly. The rings can also be made slimmer than the beams (Table 6.1 and Table 6.2), which will result in a smaller diameter of the generator. A ring is more expensive to produce, and metal-working factories for casting a 2-2.5 diameter large ring are limited. As a result of these preliminary simulations and evaluation, the ring is chosen as solution for the carrying elements for both the stator and rotor active parts.

The laminations and magnets need to be attached to both sides of the rings, and they must have the ability to slide in axially from the outside of the generator. As the small air gap makes it difficult to bolt the laminations directly to the ring, there are mainly two ways of doing this: bolting sliding tracks to the ring or mill out tracks in the ring. Manufacturing, costs, stiffness and potential stresses in the material has to be considered.

### 3.1.4 Cooling of stator

According to SmartMotor, cooling of the rotor parts will be sufficient using oil. The windings will be the main heat source, which has to be removed. In this case water will be used, and the generator needs continuous supply of cold seawater or radiators in connection with internal water flow.

### 3.1.5 Morphology of partial solutions

The rings can be fastened to the rotor base structure and to the stator walls in numerous ways. There are also different ways of designing the rotor and stator main structure,

### 3.1 Partial solutions

and the track design for the laminations. Different alternative within all these areas are shown in the morphology table (Table 3.1).

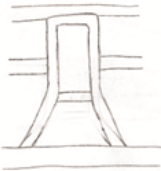
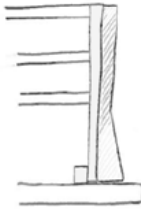
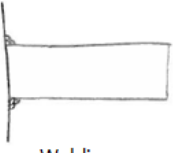
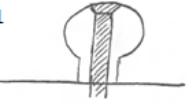

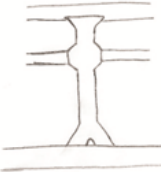
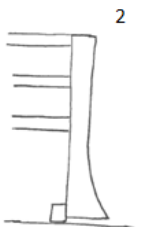
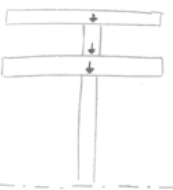
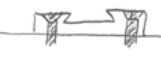


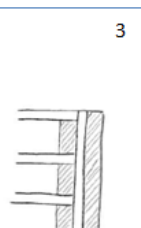
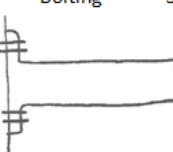



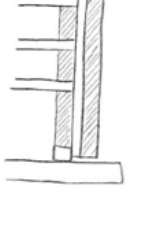









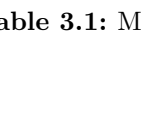
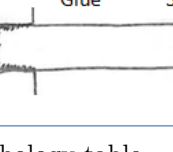


Rotor structure	Stator structure	Fastening of rings	Tracks for laminations
 1	 1	 Welding 1	1  2 
 2	 2	 Shrinking 2	3  4 
 3	 3	 Bolting 3	5  6 
 4	 3	 Shrinking 4	7  8 
 5	 3	 Glue 5	9  10 
 6	 3	 Glue 5	11  12 

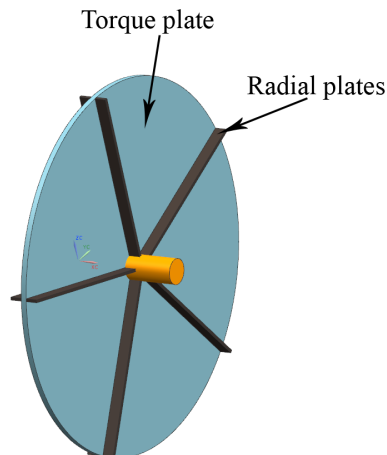
Table 3.1: Morphology table

## 3.2 Evaluation of partial solutions

### 3.2.1 Rotor main structure

To withstand tangential forces, the structure should be solid in the radial direction; from the axle and to the outer ring. Increasing the axial thickness strengthens the structure against bending from radial forces on the rings. However, using a structure which is thick in both radial and axial direction means a big, heavy structure which is costly to produce (alternative 3 and 4). Using plates to counteract bending of the rotor from the radial forces (shaded area in alternative 5 and 6, illustrated in Figure 3.5, will reduce the weight but still maintain a stiff structure. Using plates are much cheaper than casting or cut out a solid ring on the lathe. For the rotor, alternative 5 will be easier to assemble than alternative 6 because of easier access to welding zones.

**Chosen solution: Alternative 5** (Figure 3.5)



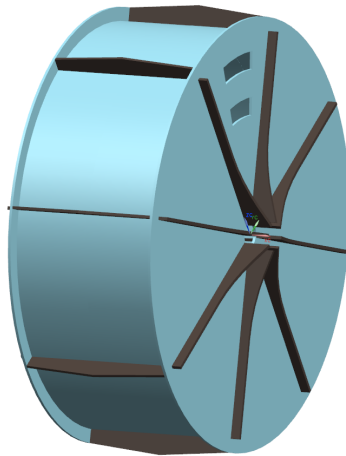
**Figure 3.5:** Chosen solution rotor structure

### 3.2.2 Stator main structure

The stator structure will consist of one outer ring and two side structures. The side structures must be strong in axial direction, especially since their load case is asymmetric because of active parts only on one side. They can be made either solid (alternative 2) or strengthened with plates (alternative 1 and 3, same principle as on the rotor structure). Using plates makes the structure stiff and light, and keeps costs down.

**Chosen solution: Alternative 1** (Figure 3.6)





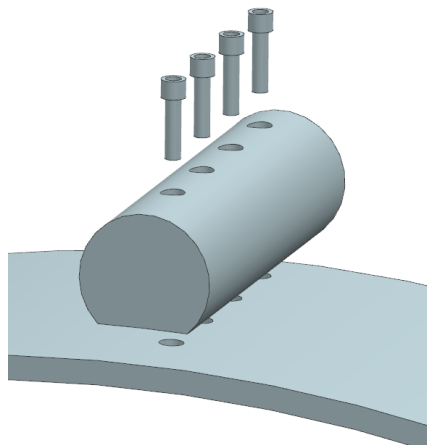
**Figure 3.6:** Chosen solution stator structure

### 3.2.3 Fastening of rings

The connection should be strong, rigid and assembly-friendly. The small air gap means that the rings have to be perfectly aligned; this becomes more important if the length of the rings is increased. Welding the ring to the rotor or stator can induce alignment issues, and once a ring is welded in place it can be difficult to adjust. Using flanges on the rings and bolt the rings in place provide better flexibility than welding. The forces which have to be absorbed per bolt can easily be reduced by increasing the number of bolts per ring. Using glue is not considered a strong enough connection. In addition it would require a thicker rotor and stator structure to compensate for the cut outs in the torque plate. Shrinking also means added thickness in the same way as for gluing. It can also cause misalignment, as with welding. Shrinking the rings in layers (alternative 2) can cause alignment problems and will be the most difficult alternative to assemble.

**Chosen solution: Alternative 3**

### 3.2.4 Tracks for laminations



**Figure 3.7:** Track bolting to a ring

The laminations need a minimum radial thickness so that the magnetic field can pass through without interference from the ring and rails. The thickness beyond this should be limited; thicker active parts mean less power output or a larger generator. The shape of the tracks or cutouts affects the manufacturing difficulties and costs. Because of the high costs and complexity of milling out tracks in the ring, alternative 11 and 12 are rejected as possible solutions. The shape of the profiles determines how well they can withstand the radial and tangential forces. A broad structure is favorable to prevent bending of the profiles. Also, it is beneficial to have a symmetrical shape so the bending of the bolts is minimized. It is also beneficial to limit the number of bolts to reduce assembly time.

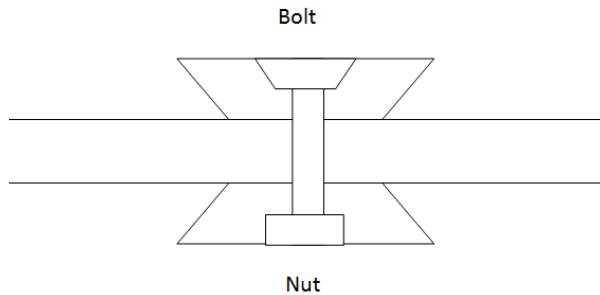
Alternative	Profile height (1-3, 1 is lowest)	Manufacturing costs (1-3, 3 is most costly)	Stiffness (1-3, 1 is stiffest)
1	3	3	2
2	1	3	1
3	2	2	1
4	1	1	3
5	2	3	1
6	3	2	2
7	3	3	1
<b>8</b>	<b>1</b>	<b>1</b>	<b>1</b>
9	2	1	2
10	3	3	3

**Table 3.2:** Evaluation of track-alternatives for a rotor/stator ring

Alternative 8 have a low profile, simple shape, only one string of bolts and can withstand radial and tangential forces well.

**Chosen solution: Alternative 8**

The bolts must be flush with the face of the rail, as the laminations are sled onto the rail (Figure 3.8).

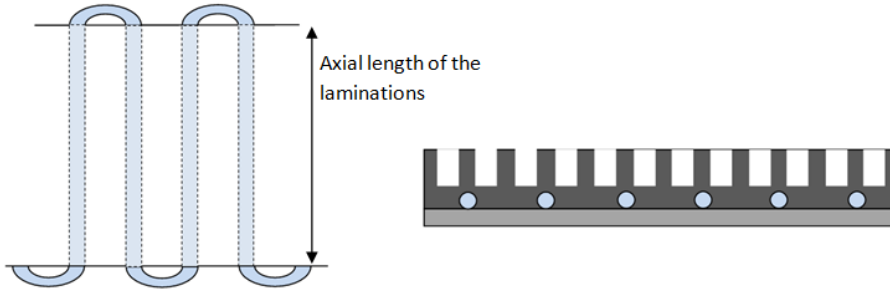


**Figure 3.8:** Solution for the rail bolt connection

### 3.2.5 Cooling of stator

As described in section 2.2, the magnet field in the laminations cannot be disrupted. Cooling channels can therefore not be placed close to the windings, but instead in cooling channels close to the stator rings. The channels can either be cut out in

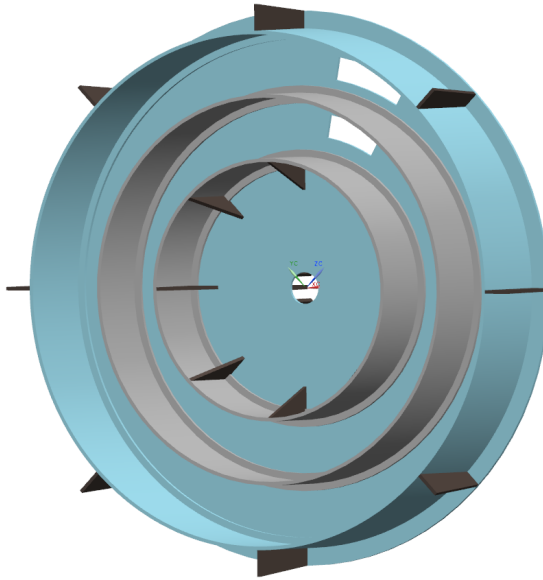
the laminations or in separate channels between the ring and lamination (which also requires corresponding cuts in the lamination). A third option is cut out channels in the ring itself, but this will be too expensive to manufacture. Channels in the lamination itself will give the best cooling, but the laminations cannot be in direct contact with the water. Using separate channels and corresponding cut outs in the lamination will be watertight and makes it easier to design transitions between the channels and the rest of the water passage.



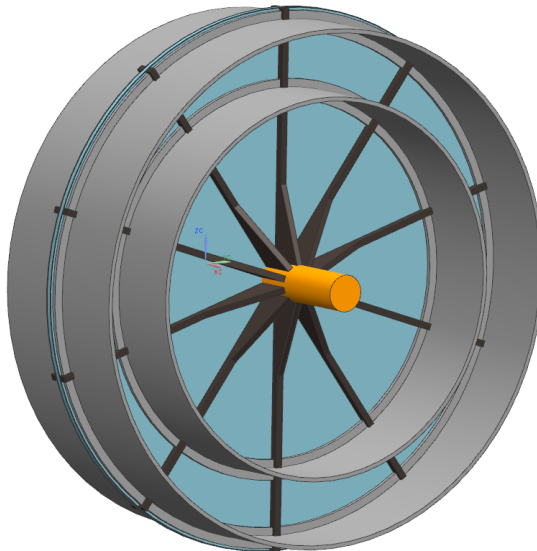
**Figure 3.9:** Chosen stator cooling solution. Cooling tubes seen in the radial direction to the left and axial direction to the right

The chosen alternative (Figure 3.9) is to use separate tubing between the ring and laminations. This means that the laminations must be shaped to fit around the tubing. The tubing should be made of a material with good heat transfer properties. The tubing will go back and forth through the lamination in the axial direction (Figure 3.9).

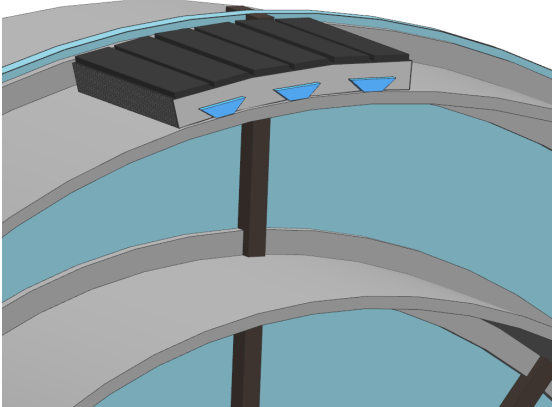
### 3.3 Chosen carrying structure solutions



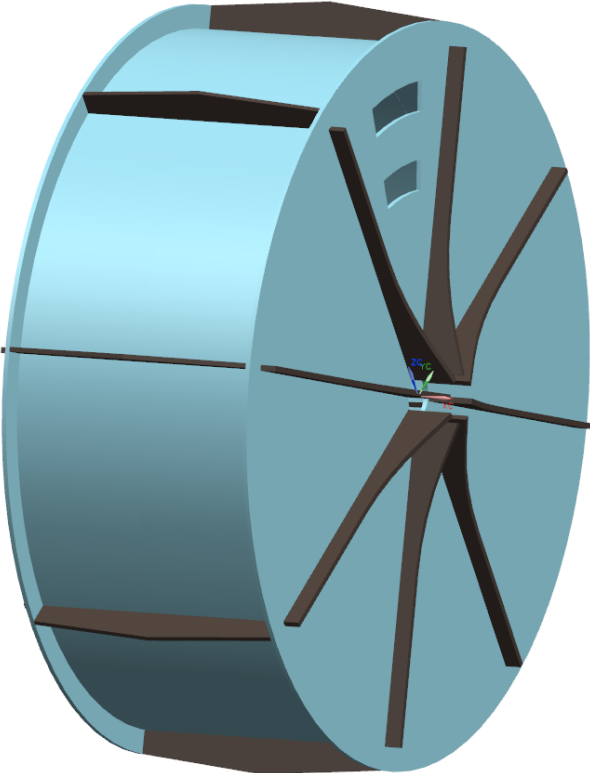
**Figure 3.10:** Stator structure with rings



**Figure 3.11:** Rotor structure with axle and rings



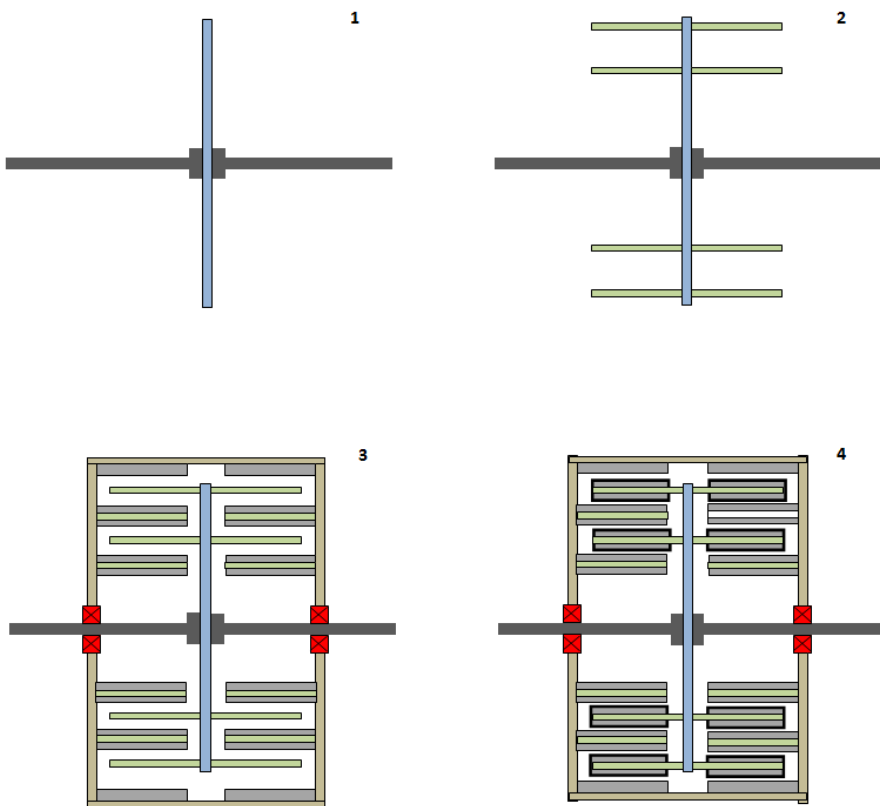
**Figure 3.12:** Segment of laminations and magnets attached to the rotor



**Figure 3.13:** Complete assembly of the generator with holes for insertion of magnet and lamination segments

#### 3.3.1 Assembly

As there are limited space between the active parts and large magnet-magnet forces, the assembly of the generator can be challenging. Because of this, the magnets and laminations are divided into sections, which makes it possible to insert the sections one by one after the complete stator is assembled (Figure 3.3). The first step of the assembly will be to bolt the rotor structure to the axle. Then bearings and both stator parts are assembled with laminations and windings. Finally the magnet and lamination segments are inserted through the stator and onto the rails on the rotor rings (Figure 3.14).



**Figure 3.14:** Assembly, step by step progress





# 4 Design and analysis

## 4.1 Objective of task

To proper design and dimension the carrying structure, static and eigenmode FEM analysis were performed. To ease the simulations, the carrying structure was divided into separate parts:

- Rotor and stator rings
- Rotor and stator structure

Load cases reflecting the worst possible case during operation were defined. The power output requirement for the generator is 1.1 MW, and this can be done with different generator dimensions. To choose the diameter and axial length of the generator, preliminary simulations were done to investigate the effect of changing these dimensions. Then final simulations were done on a carrying structure with the chosen dimensions.

## 4.2 Summary

### 4.2.1 Load cases

Part	Load case	Comment
Inner rotor ring	LC1	Normal operation vs stator short circuit
Outer rotor ring	LC1	Normal operation vs stator short circuit
Inner stator ring	LC2, LC3	Normal operation and stator short circuit
Middle stator ring	LC1	Normal operation vs stator short circuit
Outer stator ring	LC2, LC3	Normal operation and stator short circuit
Rail	LC4	Estimated worst case during normal operation
Rotor structure	LC5, Eigenmode	Simplified worst case simulation, eigenmode simulation
Stator structure	LC5, Eigenmode	Simplified worst case simulation, eigenmode simulation
Complete generator	LC6	Lifting scenario

**Table 4.1:** Load cases used for each part

### 4.2.2 Tools

The modeling and simulations were performed in NX 7.5 and NX Nastran 7.5.

### 4.2.3 Materials

Component part	Material
Rings	AISI 304L
Torque plates	AISI 304L
Rails	AISI 304 1/4 hard

**Table 4.2:** Suggested material for the parts of the carrying structure

### 4.2.4 Results

Component part	Load case	Stress amplitude incl. corr factors [MPa] (elemental)	Fatigue limit (131 MPa / 243MPa) utilization factor
Inner rotor ring	LC1	4.9	$4.9/131 = 0.037$
Outer rotor ring	LC1	2.8	$2.8/131 = 0.021$
Inner stator ring	LC2	10.6	$10.6/131 = 0.081$
	LC3	7.6	$7.6/131 = 0.058$
Middle stator ring	LC1	3.3	$3.3/131 = 0.025$
Outer stator ring	LC2	11.6	$11.6/131 = 0.089$
	LC3	11.0	$11.0/131 = 0.084$
Rail	LC4	140.3	$140.3/243 = 0.577$

**Table 4.3:** Final simulations of the rings and rail, FLS results

Component part	Load case	Von Mises stress, incl. corr factors [MPa] (elemental)	(ULS) Yield strength utilization factor	Lowest eigenmode [Hz]	Eigenmode limit safety factor
Rotor structure	LC5	13.3	0.07	45.7	$45.7/43.2 = 1.06$
Stator structure	LC5	11.0	0.06	45.7	$45.7/41.1 = 1.11$
Complete generator	LC6	181.1	0.095	-	-

**Table 4.4:** Final simulations of the rotor and stator assembly, ULS and ELS results

### 4.3 Design

The final design of the generator is shown in figures below. Power output calculation for the final design is shown in Appendix F - chapter 11.

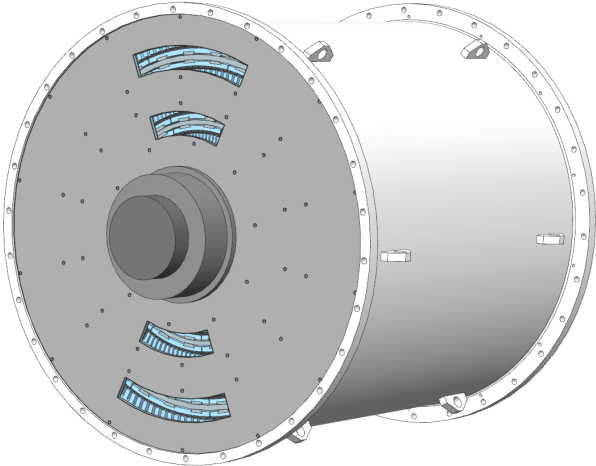


Figure 4.1: Final generator

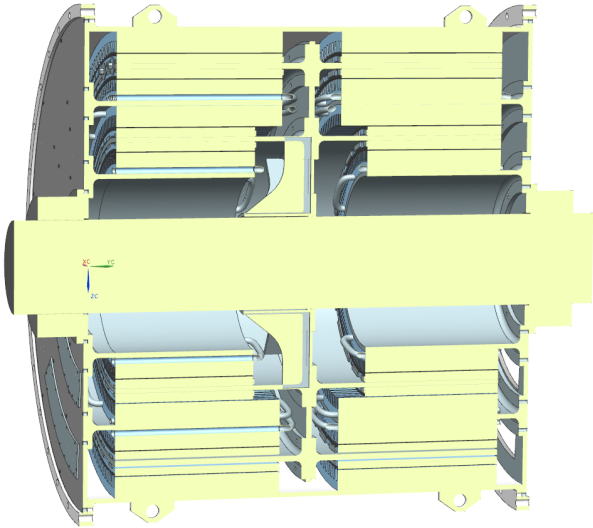
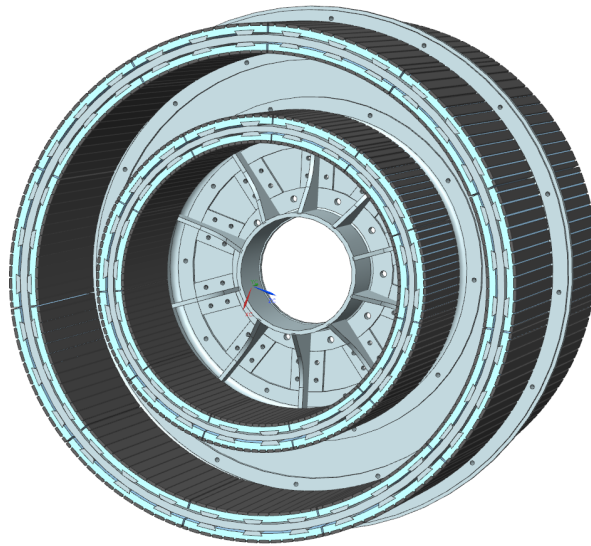
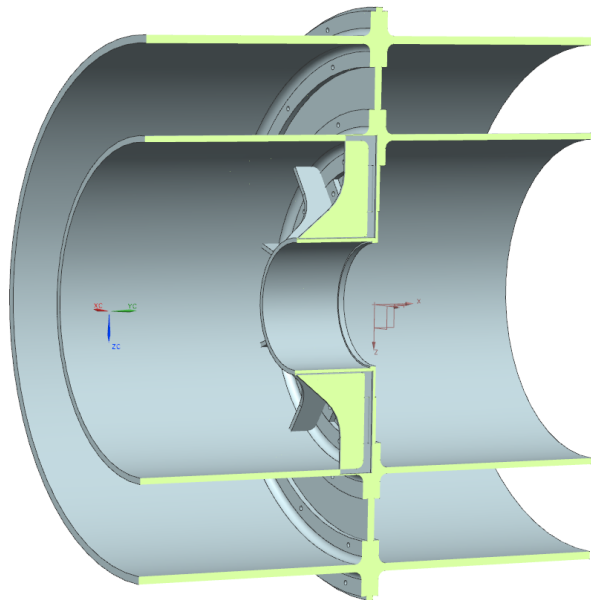


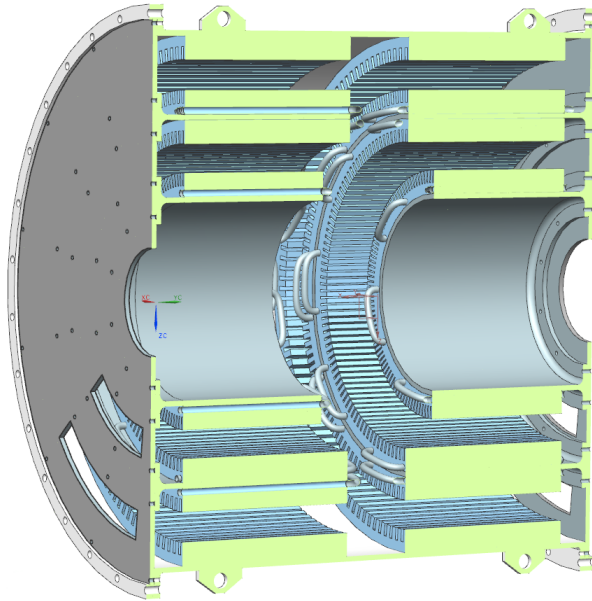
Figure 4.2: Sectioned view of the generator including axle and bearings



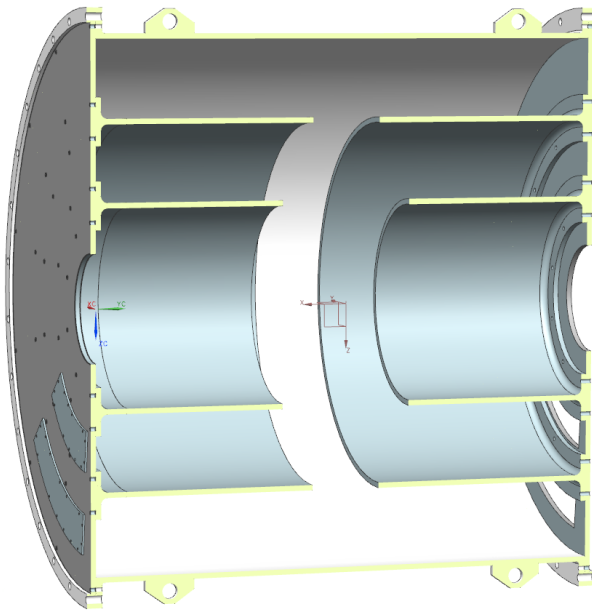
**Figure 4.3:** Rotor structure including magnet and lamination sections (11 sections per ring side)



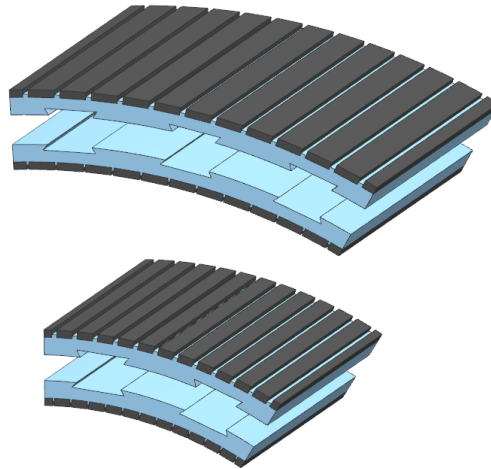
**Figure 4.4:** Sectioned view of the rotor structure



**Figure 4.5:** Sectioned view of the stator including active parts and cooling tubes



**Figure 4.6:** Sectioned view of the stator structure



**Figure 4.7:** Magnets and lamination sections for outer and inner rotor ring. 12 magnets per sections. 3 rails per section for outer rings and 2 rails for inner rings

### 4.3.1 Ring dimensions

The dimensions of the rings including laminations and active parts are shown in Figure 4.8 and Figure 4.9. Exact geometry values and weight are listed in Table 4.5 and Table 4.6.

Ring	Diameter [mm]	SSL [mm]	Weight ring [kg]	Weight rails [kg]	Weight active parts [kg]
Inner rotor ring	1077	610	533	90	655
Outer rotor ring	1704	730	957	162	1245
Inner stator ring	766	610	335	-	693
Middle stator ring	1388	730	689	-	3043
Outer stator ring	2020	2x730	2429	-	4449

**Table 4.5:** Ring dimensions and weight. There are two of each ring except the outer stator ring

Ring dimensions	
Measure	[mm]
MH	10
LTR	15
RT	15
CDT	30
LTS	60.5
FH	180
FT	20
FML	55
EWL / EWL (inner rotor ring)	100 / 220
Ring thickness / Ring thickness outer rotor ring	20 / 25
Outer stator ring flange dimensions	Figure 4.9

Table 4.6: Ring dimensions

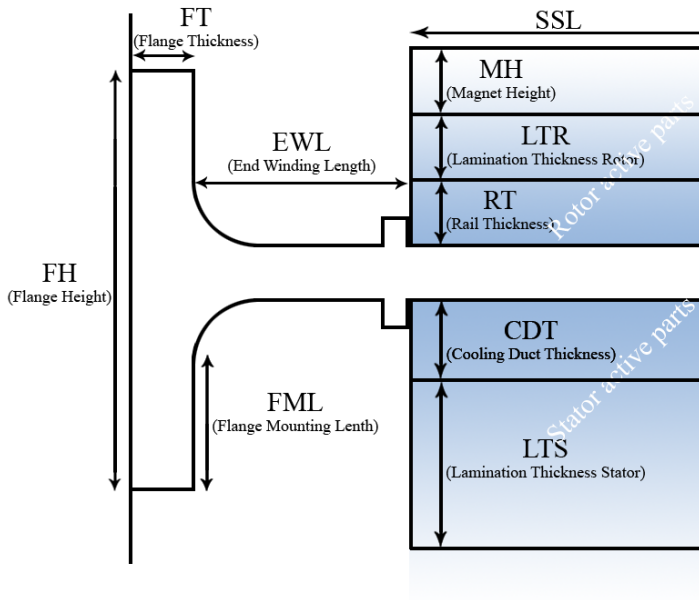


Figure 4.8: Ring, flange and active parts dimensions



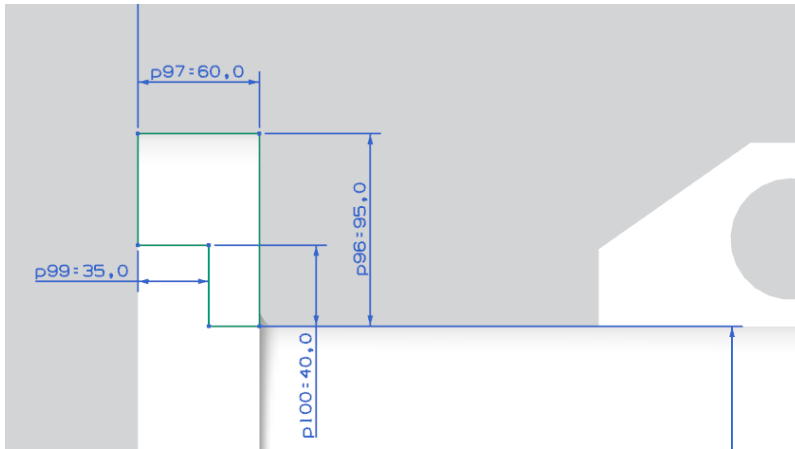


Figure 4.9: Outer stator ring flange dimensions

## 4.4 Rotor and stator structure material data

### 4.4.1 Material properties

All materials in contact with the laminations are required to be non-magnetic. The only relevant material for this generator is austenitic stainless steel from the 200- or 300-series. Chosen material for the rotor and stator structure, including the rings but excluding the rails, is stainless steel AISI 304L. This is a material with high stiffness, relatively high strength and is suited for casting, rolling, machining and welding. A higher strength is needed for the rails because of increased stresses. The chosen material for the rails is stainless steel 304 1/4 hard, which means it is cold rolled for increased strength. The material data are taken from CES EduPack 2011 [3]. The complete data sheet is found in Appendix C (chapter 8).

Material	Application	Young's modulus, E [GPa]	Poisson's ratio, $\nu$	Density, $\rho$ [kg/m <sup>3</sup> ]	Tensile strength, $R_m$ [MPa]	Yield strength, $R_{p0,2}$ [MPa]
AISI 304L	Rings, rotor and stator structure	205	0,3	7950	480*	190*
AISI 304 1/4 hard	Rails	205	0,3	7950	860*	515*

Table 4.7: Material data for rotor and stator structure

\* *Lowest values from CES EduPack*

The laminations are made of many thin sheets of steel and gives the ring additional stiffness, but the adhesion between the laminations are weaker than in an isotropic material. No material data was available on the laminations, but instead estimated as an orthotropic material as shown below:

Stiffness parameter	Young's modulus, E [GPa]
$E_1$ axial direction	50 GPa
$E_2$	200 GPa
$E_3$	200 GPa
$G_{12}$	20 GPa
$G_{13}$	20 GPa
$G_{23}$	80 GPa

**Table 4.8:** Lamination material properties in NX

#### 4.4.2 Fatigue properties

Material	Fatigue limit amplitude (N = $10^7$ , R=-1), $\sigma_A$ [MPa]	Fatigue limit range (N = $10^7$ , R = 0), $\Delta\sigma_R$ [MPa]
AISI 304L	131	150
AISI 304 1/4 hard	192	243

**Table 4.9:** Fatigue properties from CES EduPack

The estimated stress cycles for the generator are above  $10^7$ . By assuming no failure beyond  $N = 10^7$ , the fatigue limits from Table 4.9 are used as upper stress limits in all simulations.

## 4.5 Safety factors

### 4.5.1 ULS safety factor

It is decided to define all parts simulated in this report as critical to failure, meaning failure of one component will lead to failure of a major part of the generator. The main reason for this is the small air gap (5mm) between the stator and the moving rotor. According to IEC 61400-1:2007 [4], the consequence of failure factor,  $\gamma_n$ , is 1,0.

The total required ULS safety factor becomes:

$$S_{f,ULS} = \gamma_m \cdot \gamma_n = 1,1 \cdot 1,0 = \mathbf{1,1} \quad (4.1)$$

where

$\gamma_m$  = partial material factor (Appendix D (chapter 9))

### 4.5.2 ULS safety factor - lifting

During assembly, installation and maintenance the generator will be lifted. According to Standard No. 2.7-3 - Portable offshore units [5], a safety factor of 2.5 multiplied to the maximum gross weight (MGW) shall be used. This standard is made for the oil and gas industry, but is relevant for this case as well.

$$S_{f,ULS-lifting} = \mathbf{2.5} \quad (4.2)$$

### 4.5.3 FLS safety factors

The following safety factors for FLS are calculated in Appendix D (chapter 9):

Safety factor	Abbr.	Code	Calculated value
Surface finish	$f_s$	EN 13445-6:2009 [6]	0,90/0,86/0,83*
Wall thickness	$f_e$	EN 13445-6:2009	1
Temperature	$f_t$	EN 13445-6:2009	1
Mean stress	$f_m$	EN 13445-6:2009	1
Partial material	$\gamma_m$	IEC 61400-4 [4]	1,1
Consequence of failure	$\gamma_n$	IEC 61400-1	1,0

**Table 4.10:** FLS safety factors

\* Values listed for: AISI 304L, machined / AISI 304L, rolled / AISI 304 1/4 hard, machined

The total safety factor defined in Appendix D (chapter 9) is given by:

$$S_{f,FLS} = \frac{\gamma_m \cdot \gamma_n}{f_s \cdot f_e \cdot f_t \cdot f_m} \quad (4.3)$$

For the different materials and production method, the total safety factor becomes:

#	Material	$S_{f\#,FLS}$
1	AISI 304L, machined	1,22
2	AISI 304L, rolled	1,28
3	AISI 304 1/4 hard, machined	1,33

**Table 4.11:** Surface finish factor

The effective stress notch amplitude is

$$\sigma^* = S_{f,FLS} \cdot \sigma_{eq,struct} \quad (4.4)$$

and the effective stress notch range is

$$\Delta\sigma^* = S_{f,FLS} \cdot \Delta\sigma_{eq,struct} \quad (4.5)$$

where  $\sigma_{eq,struct}$  is the structural stress amplitude (for R = -1) and  $\Delta\sigma_{eq,struct}$  is the structural stress range (for R = 0) calculated by FEA.

The effective notch stress amplitude (or range) is compared to the fatigue limit amplitude (or range).

## 4.5.4 ELS safety factors

### 4.5.4.1 Rotor structure

The forces from the rotor-stator interaction vary with a frequency of 26.4 Hz at normal operating speed. To avoid any resonance, the rotor was analyzed for potential eigenfrequencies. To make sure the rotor does not come close to any of the eigenfrequencies, a safety factor of 1.7 compared to the force frequency was set:

$$S_{fR,ELS} = 1.7 - \text{equals a maximum allowed frequency of 43.2 Hz}$$

### 4.5.4.2 Stator structure

The forces from the rotor-stator interaction vary with a frequency of 24.2 Hz at normal operating speed. The lower frequency limit was set to two times the normal operating frequency:

$S_{fS,ELS} = 1.7$  - equals a maximum allowed frequency of 41.1 Hz

## 4.6 Load cases

All force values comes from calculations done by SmartMotor on an air gap with diameter of 2665.5mm, which is bigger than the air gaps on this generator. This makes the simulations conservative, as a smaller diameter means smaller or fewer magnets. The sinusoidal force parameters are calculated according to equations in section 2.4 and shown in tables below. The exact forces used in the simulations are calculated according to Equation 2.6.

Input parameters for the force curves		
	Rotor ring	Stator ring
Frequency	152.1 rad/s	165.9 rad/s
Phase difference	0.57 rad	0.52 rad

**Table 4.12:** Frequency and phase difference

Radial force parameters, normal operation, 3mm air gap	
Amplitude 1	3843 N/m
Amplitude 2	4213 N/m
Amplitude 3	5102 N/m
Amplitude 4	3690 N/m
Center value 1	9562 N/m
Center value 2	11630 N/m
Center value 3	12583 N/m
Center value 4	10947 N/m

**Table 4.13:** Normal operation force parameters, 3mm air gap. Force values are for each tooth/magnet per meter in the axial direction

Radial force parameters, short circuit	
Amplitude 1 (3mm air gap)	1806 N/m
Amplitude 2 (3mm air gap)	1801 N/m
Center value 1 (3mm air gap)	12009 N/m
Center value 2 (3mm air gap)	12132 N/m
Max Amplitude (7mm air gap)	1604 N/m
Max Center value (7mm air gap)	5556 N/m

**Table 4.14:** Radial forces. Short circuit force parameters, 3mm air gap. Force values are for each tooth/magnet per meter in the axial direction

Tangential force parameters, normal operation, 3mm air gap	
Amplitude 1	2814 N/m
Amplitude 2	2834 N/m
Amplitude 3	3577 N/m
Amplitude 4	2708 N/m
Center value 1	1819 N/m
Center value 2	1449 N/m
Center value 3	1685 N/m
Center value 4	1531 N/m

**Table 4.15:** Tangential forces. Normal operation parameters. Force values are for each tooth/magnet per meter in the axial direction

## 4.6.1 Load cases for rings

### 4.6.1.1 LC1, LC2 and LC3

Forces generated by the rotor-stator interaction have been simplified as sinusoidal force curves (equations are shown section 2.4). The exact force curve parameters are tabulated in Table 4.12, Table 4.13, Table 4.14 and Table 4.15. Both rotor rings and the middle stator ring have active parts on both sides. This means that during normal operation the radial forces are symmetrical, and the rings will not be tested for this load case. A load case with normal operation on one side and stator short circuit forces on the other side is the worst case scenario (LC1). Inner and outer stator rings have only active parts on one side, and both a normal operation (LC2) and stator short circuit (LC3) load case were tested. These load cases consists of oscillating forces and the results from the simulations must be compared to the FLS stress limit. A summary of the load cases for the rings are listed below:

**LC1:** Normal operation vs short circuit

- Inner and outer rotor rings
- Middle stator ring

**LC2:** Normal operation, **LC3:** Short circuit

- Inner and outer stator rings

### 4.6.1.2 LC4 - Rails

Each rail on the outer rotor rings holds four magnets lines, while the rails on the inner rings holds six. The maximum force a magnet row can achieve is 18000 N/m (axial length). The maximum force for each rail is calculated below:

$$F_{r-inner} = 6 \cdot 18000 \frac{N}{m} \cdot SSL [m] \quad (4.6)$$

$$F_{r-outer} = 4 \cdot 18000 \frac{N}{m} \cdot SSL [m] \quad (4.7)$$

\* *SSL*: Axial length of the active parts

These forces were used for the rails on both the inner and outer rings. As the magnets will not achieve the maximum value at the same time, this estimate is conservative.

Ring location	SSL [m]	F <sub>r</sub> [N]
Outer rotor rings	0,73	52560
Inner rotor rings	0,61	65880

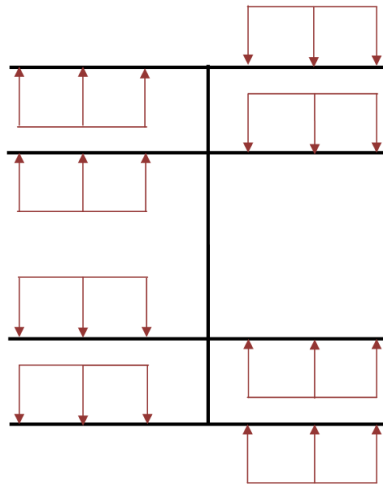
**Table 4.16:** Forces on each rail

## 4.6.2 Rotor and stator structure assembly

### 4.6.2.1 LC5

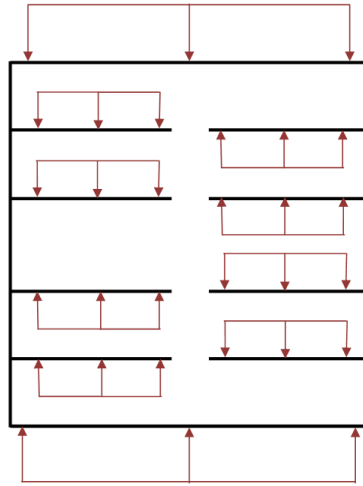
Analyzing the rotor and stator structures with all the rings and the correct forces in place is too time consuming (a total of 2064 individual forces) and will most likely be too complex for the available computers to handle. Instead, the structures were analyzed with a simplified, but worse, load case (Figure 4.10 and Figure 4.11).

The direction of the forces acting on each ring is chosen to make the total load case as unsymmetrical as possible, and is shown below:



**Figure 4.10:** Worst case load, rotor main structure





**Figure 4.11:** Worst case loads, stator main structure

A summary of the forces, as a function of SSL, is shown in the table below:

Force	Part	Magnitude
Normal operation vs short circuit*	Inner rotor ring	4000N·SSL[m] per magnet or stator tooth
	Outer rotor ring	
	Middle stator ring	
Normal operation on one side of ring	Inner stator ring	18000N·SSL[m] per magnet or stator tooth
	Outer stator ring	
Weight of active parts	All rings	Estimated by SmartMotor (Appendix E, chapter 10)

**Table 4.17:** Rotor structure forces

\* Attraction forces between rotor and stator, difference between maximum force in normal operation and minimum force for short circuit case. Valid for rings with active parts on both sides.

#### 4.6.2.2 LC6

As the generator is going to be lifted through lifting points on the stator, the stator must be able to hold the whole weight of the generator. When lifted, the weight of the rotor and axle will be resting on the center holes of the two stator torque plates. Weight estimations of the stator, rotor and axle structure are taken from NX and the weight of laminations and magnets have been estimated by SmartMotor. All the weight estimations are found in Appendix E (chapter 10).

- Weight generator carrying structure including active parts:

- $25356\text{kg} = 248742\text{ N}$

- Axle\*:

- $2398\text{kg} = 23524\text{ N}$

*\* The weight of the axle is just an estimate, as the axle not is exactly designed. The estimate was done with a smooth axle with diameter of 400mm and length equal of the axial length of 2400mm.*

- Total weight estimate for the generator: 272266 N

There are several smaller parts which not were included in the above weight estimate: bolts and nuts, cooling system, electronics, oil and bearings. As a result of this, the total weight of the generator was increased with 10000 N, which gave a total weight of 257751 N. With the safety factor of 2.5 (subsection 4.5.2) the total weight used in the simulations was: **680666 N**.

## 4.7 Simulation setup

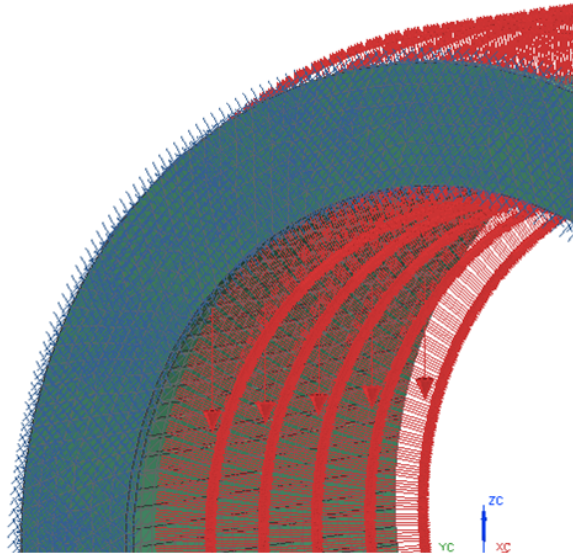
### 4.7.1 Rings simulation setup

The settings for the ring simulations in NX are shown below:

- Iterative solver: On
- Solution type: SESTATIC 101 - single constraint
- Mesh type: CTETRA(10)
- Mesh size: 50 mm
- Surface Curvature Based Size Variation: 50
- Material
  - Rings: AISI 304L (Table 4.7)
  - Rails and Laminations: Estimated lamination material (Table 4.8)

The laminations on the stator is shrunk onto the rings. In the FE model, this connection was simulated using mesh mating between the face of the ring and the adjoining face of the lamination. The rotor laminations are sled onto the ring via rails. The rails are united to the laminations and mesh mating are used between the rails and the ring. The rails are given the same material properties as the laminations because of the tolerances in the interface between the laminations and rails.

The rings are connected to the main structure of the stator and rotor via bolts through a flange. In the simulations of the rings the flange was fixed by using fixed constraint. The forces are inserted on the laminations, in each single rotor magnet slot or stator tooth. The load cases for the different rings are shown in subsection 4.6.1.



**Figure 4.12:** Fixed constraint and forces on the stator ring simulation model

## 4.7.2 Rotor and stator structure simulation setup

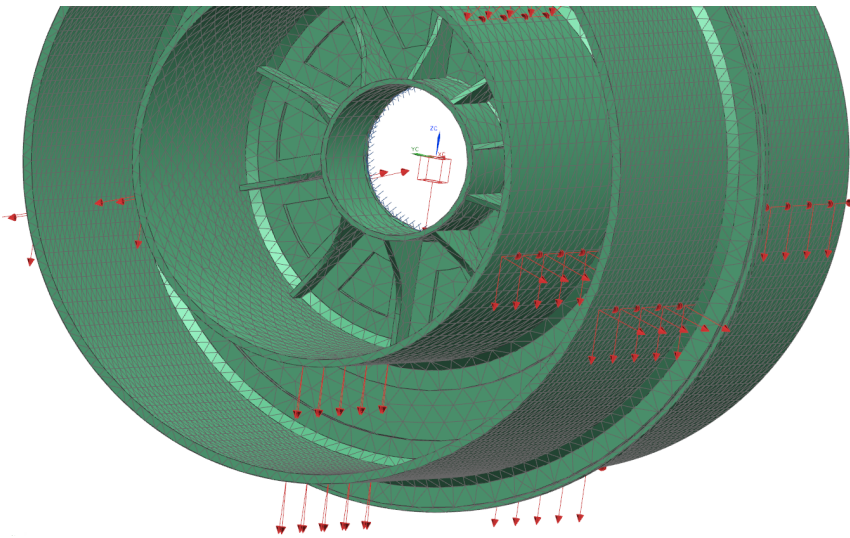
The settings for the rotor and stator structure simulations in NX are shown below:

- Iterative solver: On
- Solution type:
  - Static simulations: SESTATIC 101 - single constraint
  - Eigenmode simulations : SEMODES 103 - Flexible Body
- Mesh type: CTETRA(10)
- Mesh size: 60 mm
- Surface Curvature Based Size Variation: 50
- Material: AISI 304L (Table 4.7)

Both the rotor and stator rings are directly connected to the torque plates. This means that the forces acting on the rings will affect the deformations on the rotor and stator torque plates.

### 4.7.2.1 Rotor structure assembly

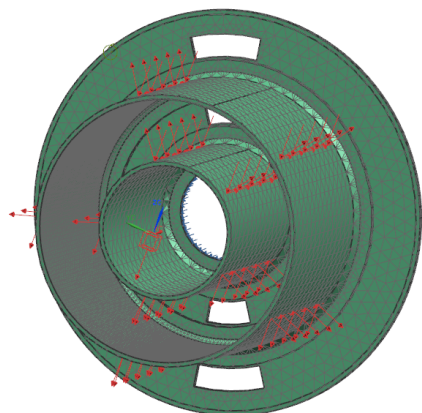
The rotor torque plate was united with outer and inner rotor rings, and the forces attached to the outer or inner sides. The rotor was constrained using fixed constraint at one side of the torque plate, where the axle will be bolted in. The model was analyzed without the laminations, but this only made the simulations slightly conservative in terms of deformations and stresses. Constrains and forces are shown in Figure 4.13. The weight of the structure was included using gravity function in NX. The weight of the active parts was included by inserting an evenly distributed unidirectional force for each ring.



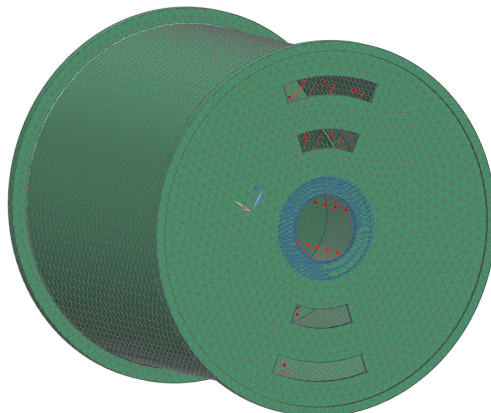
**Figure 4.13:** Simulation model rotor main structure

### 4.7.2.2 Stator structure assembly

The stator structure is fixed around the holes at the center of each torque plate, where the structure bolts to the bearing housings. As on the rotor structure assembly the laminations were left out. Constraints and forces are shown in Figure 4.14 and Figure 4.15.



**Figure 4.14:** Stator simulation setup - forces applied to inner and middle stator rings



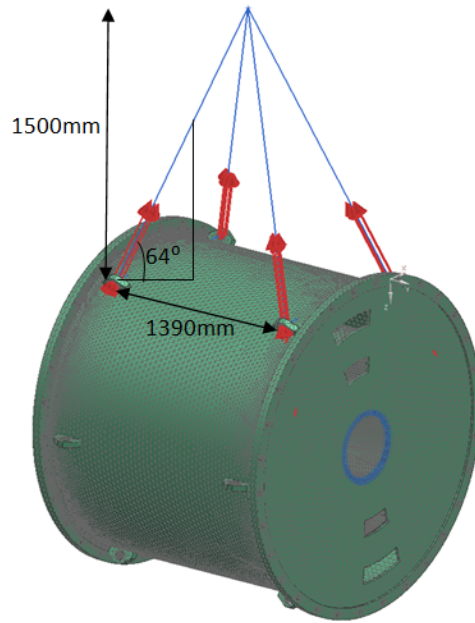
**Figure 4.15:** Stator simulation setup - fixed constrain on torque plate

### 4.7.3 Lifting scenario simulation setup

The settings for the lifting simulation in NX are shown below:

- Solution type: SESTATIC 101 - single constraint
- Iterative solver: On
- Mesh type: CTETRA(10)
- Mesh size: 40 mm
- Surface curvature based size variation: 90
- Material: AISI 304L (Table 4.7)

The center hole of the stator torque plates were fixed using fixed constraint, while the weight estimate of the whole generator with a safety factor (subsection 4.5.2) was divided between 4 lifting points. The placement of the lifting points and the lifting setup can be seen in figure (Figure 4.16).



**Figure 4.16:** Lifting simulation setup

The forces acting in each lifting point is one fourth of the total weight estimate. As the weight estimate is in the vertical direction (subsubsection 4.6.2.2), decomposition was done to find the resultant in each lifting point and calculations are shown below:

Vertical lifting force in each point

$$\frac{680666N}{4} = 170166N \quad (4.8)$$

Decomposition in the force direction gives the value

$$F_r = \frac{170166N}{\sin(64^\circ)} = 189328N \quad (4.9)$$

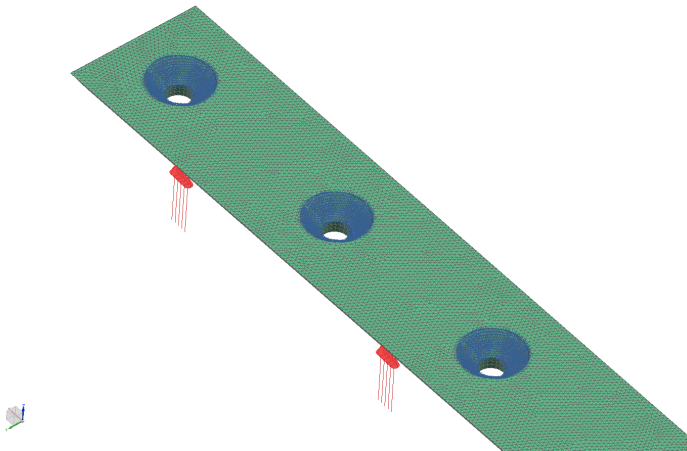
#### 4.7.4 Rail simulation setup

The settings for the rail simulations in NX are shown below:

- Solution type: SESTATIC 101 - single constraint
- Mesh size: 2 mm

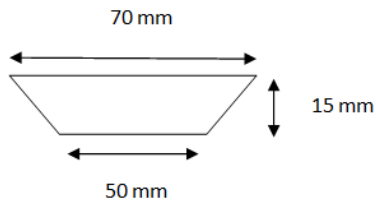
- Surface curvature based variation: 90
- Material: Steel ( $E = 207 \text{ GPa}$ )
- Holes (*countersunk*):
  - C-sink diameter: 30 mm
  - C-sink angle: 90 deg
  - Diameter: 16 mm

The rail were constrained using fixed constraint along the countersunk part of each hole, and the force was distributed along the two sloping faces of the rail (Figure 4.17).



**Figure 4.17:** Mesh, constraints and forces in rail simulation

The dimensions used are shown in figure (Figure 4.18).



**Figure 4.18:** Shape and dimensions of the rail



## 4.8 Summary of preliminary static and eigenmode simulations

In the simulations, the effect of different diameters and axial lengths were analyzed. All preliminary results are found in Appendix B - section 7.1.

All tested rings had a thickness of 20mm, but different diameters and axial lengths. The results showed that smaller diameters and longer axial lengths did not increase the deformations. The rings will only deform to a certain limit, independently of their length.

The simulations of the rotor and stator structure showed that increased axial length of the rings gave reduced deformations and stresses. The main reason for this is that the torque plates gets stiffer as the diameter decreases. This is positive as a generator with a small diameter is preferable (section 2.1). However, a smaller diameter also reduces the free space in the generator, making it harder to remove the heat. Because of these space limitations, the longest possible axial length of the active parts for the rings (SSL) was about 700mm (using 4 air gap layers).

An alternative configuration could be to eliminate the inner air gap (removing the inner stator rings) as it only produces about 100 kW (chapter 11). The axial length would have to be increased by about 0.2m, or the diameter by about 0.1m. Eliminating these rings would result in more free space. However, this would reduce the stiffness of the stator structure, as the rings stiffens the stator torque plates.

The initial eigenmode simulations were done with SSL=700mm. The rotor structure was initially not stiff enough, and stiffening plates were added in addition to increasing the thickness of the outer ring and the torque plate. To maintain the power output, these modifications altered SSL to 730mm for the outer rings and 610mm for the inner rings to make room for the stiffening plates. The stator structure was approved without modifications. The eigenmode simulations resulted in SSL=730/610mm for the final generator design.

## 4.9 Final simulations

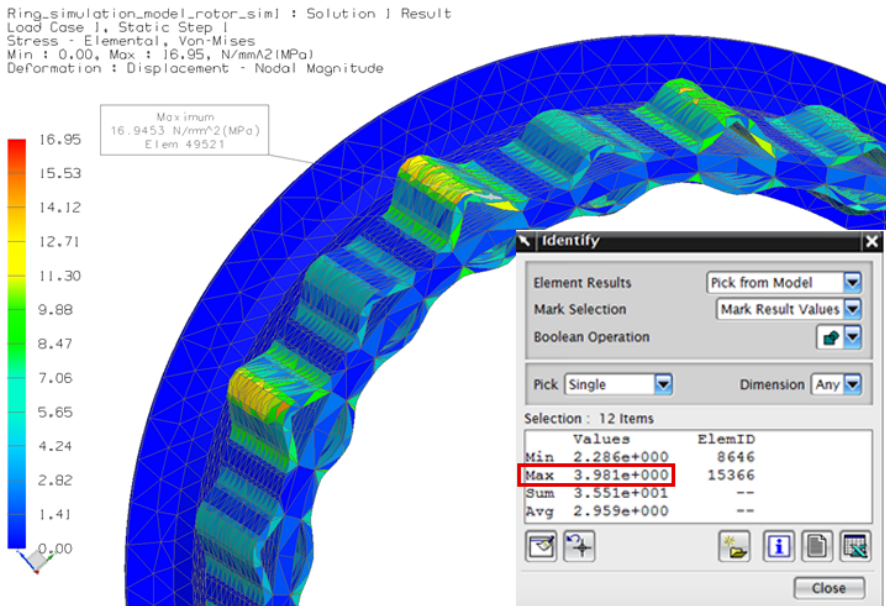
### 4.9.1 FLS results

#### 4.9.1.1 Inner rotor ring

Static simulation				
Load case	Von mises stress elemental [MPa]	Displacement [mm]	Stress amplitude incl. - corr. factors (1.22) [MPa]	Fatigue limit (131MPa) utilization factor
LC1	4.0 (17.0 for the laminations)	0.008 (0.015 for the laminations)	4.9 (Ring)	4.9/131 = 0.037

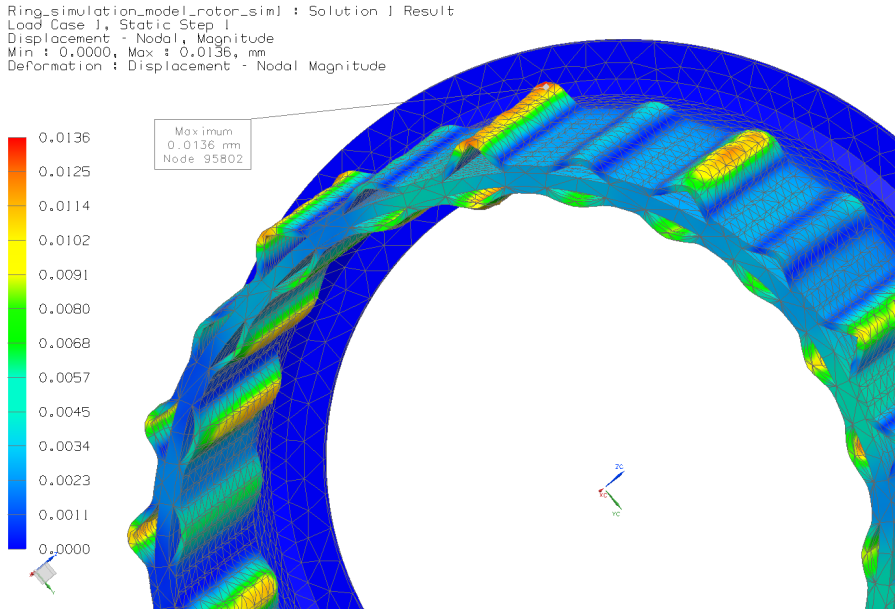
**Table 4.18:** Final results of inner rotor ring, LC1

The stresses and deformations are shown in Figure 4.19 and Figure 4.20. The laminations had higher stresses and deflections than the ring. Only 3.3% of the fatigue limit for the ring was utilized. Even though the laminations get pulled out from the ring, the deformations are small enough to be approved.



**Figure 4.19:** Inner rotor ring elemental stresses, final simulation

## 4.9 Final simulations



**Figure 4.20:** Inner rotor ring displacement, final simulation

### 4.9.1.2 Outer rotor ring

Static simulation				
Load case	Von mises stress elemental [MPa]	Displacement [mm]	Stress amplitude incl. - corr. factors (1.22) [MPa]	Fatigue limit (MPa) utilization factor
LC1	2.3 (9.7 for the laminations)	0.006 (0.015 for the laminations)	2.8	$2.8/131 = 0.021$

**Table 4.19:** Final results of outer rotor ring

The stresses and deformations are shown in Figure 4.21 and Figure 4.22. The results are similar to the inner rotor ring, where the laminations deflect more than the ring. The distance between each rail is about the same as for the inner rotor ring, because 33 rails are used instead of 22. With a fatigue limit utilization of 2.1%, the chosen design is approved.

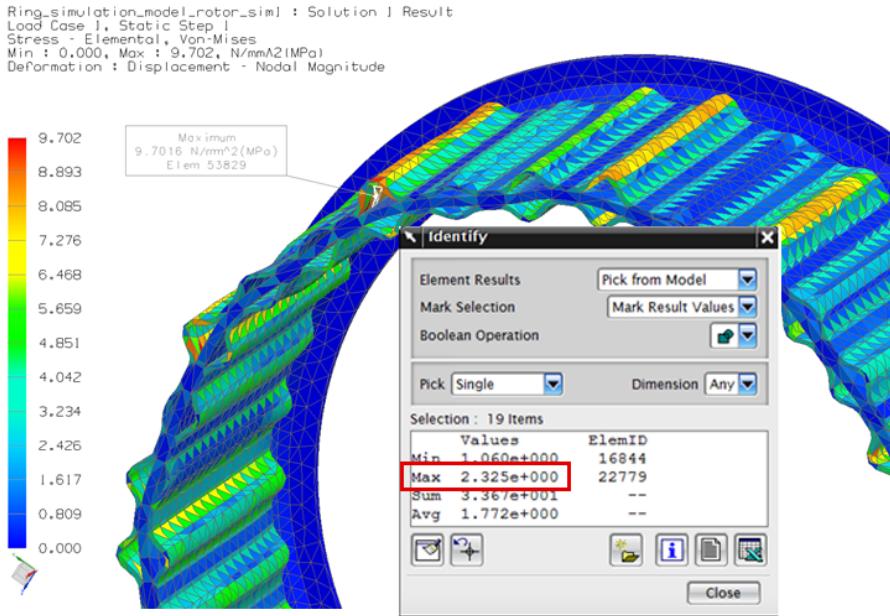


Figure 4.21: Outer rotor ring elemental stresses, final simulation

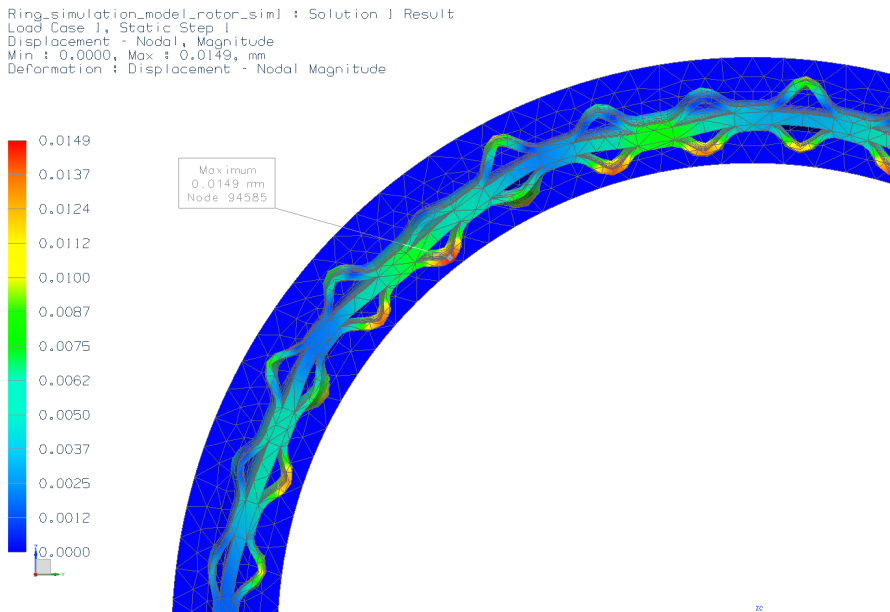


Figure 4.22: Outer rotor ring displacement, final simulation

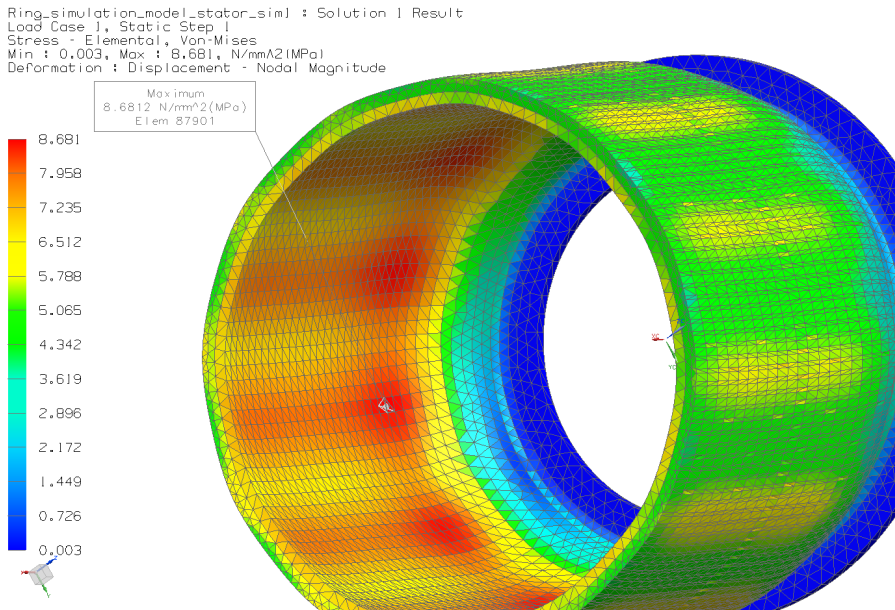
## 4.9 Final simulations

### 4.9.1.3 Inner stator ring

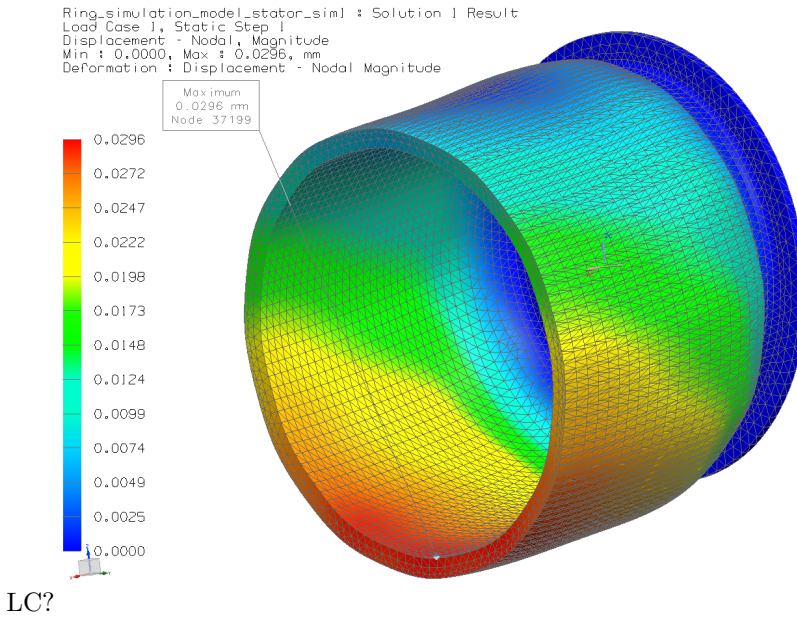
Static simulation				
Load case	Von mises stress elemental [MPa]	Displacement [mm]	Stress amplitude incl. - corr. factors (1.22) [MPa]	Fatigue limit (131MPa) utilization factor
LC2	8.7	0.030	10.6	$10.6/131 = 0.081$
LC3	6.2	0.023	7.6	$7.6/131 = 0.058$

**Table 4.20:** Final results of inner stator ring

Here the peak stresses were located on the ring and not in the laminations, which was the case for both rotor rings. Stresses are illustrated in Figure 4.23. Figure 4.24 shows that the weight of the structure contributes to the displacement. The chosen design is approved.



**Figure 4.23:** Inner stator ring elemental stresses, final simulation LC2



**Figure 4.24:** Inner stator ring displacement, final simulation LC2

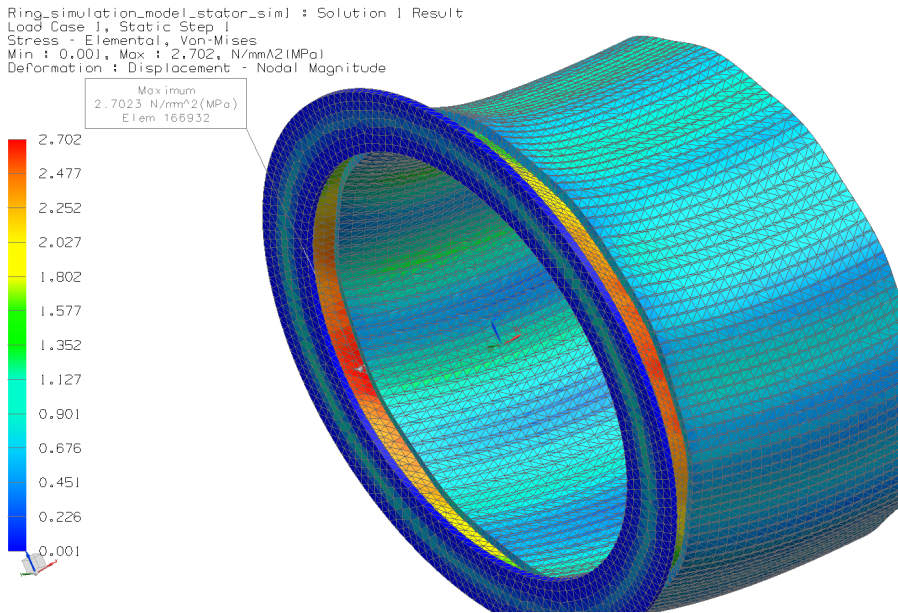
**4.9.1.4 Middle stator ring**

Static simulation				
Load case	Von mises stress elemental [MPa]	Displacement [mm]	Stress amplitude incl. - corr. factors (1.22) [MPa]	Fatigue limit (131MPa) utilization factor
LC1	2.7	0.010	3.3	3.3/131 = 0.025

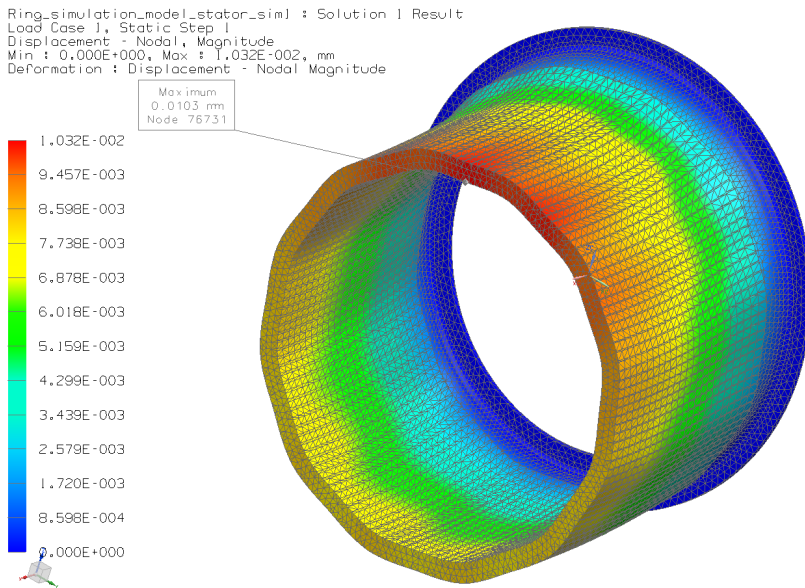
**Table 4.21:** Final results of middle stator ring

As there are forces on both sides of this ring, the total load case is easier on the ring. As a result, the peak stress location is located on the ring between the flange and laminations. Figure 4.25 shows that the weight of the structure contributes to the displacement. The chosen design is approved.

## 4.9 Final simulations



**Figure 4.25:** Middle stator ring elemental stresses, final simulation



**Figure 4.26:** Middle stator ring displacement, final simulation

4.9.1.5 Outer stator ring

Static simulation				
Load case	Von mises stress elemental [MPa]	Displacement [mm]	Stress amplitude incl. - corr. factors (1.22) [MPa]	Fatigue limit (131MPa) utilization factor
LC2	9.5 (10.0 for the laminations)	0.040	11.6 (Ring)	$11.6/131 = 0.089$
LC3	9.0 (11.0 for the laminations)	0.047	11.0 (Ring)	$11.0/131 = 0.084$

Table 4.22: Final results of outer stator ring

The outer stator ring stretches between the two torque plates. Normal operation load case proved to be the worst and the fatigue limit utilization factor is 8.9%. As this ring have active parts on only the inside, the structure deforms inwards. Stresses and displacement are shown in Figure 4.21 and Figure 4.28. The chosen design is approved.

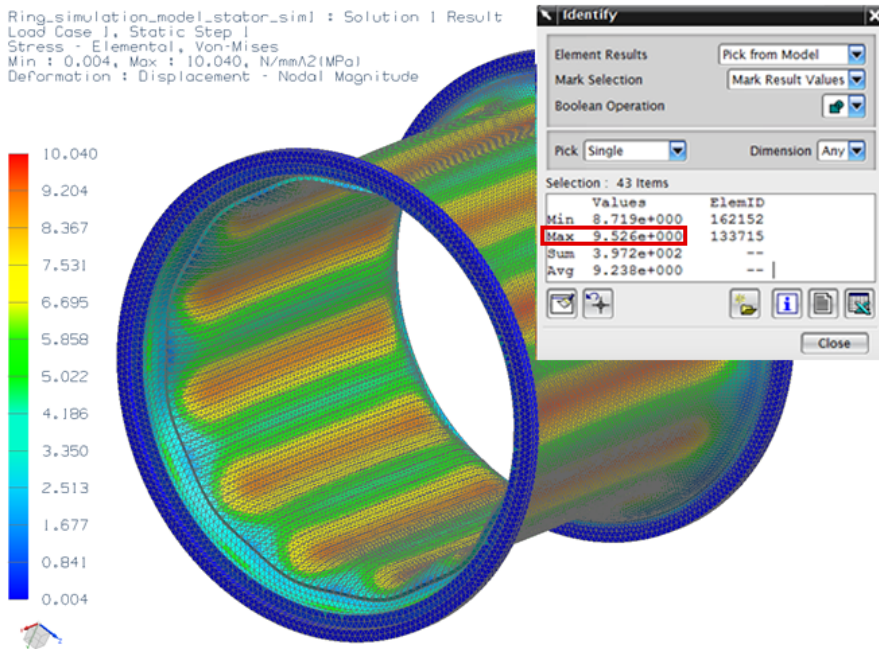
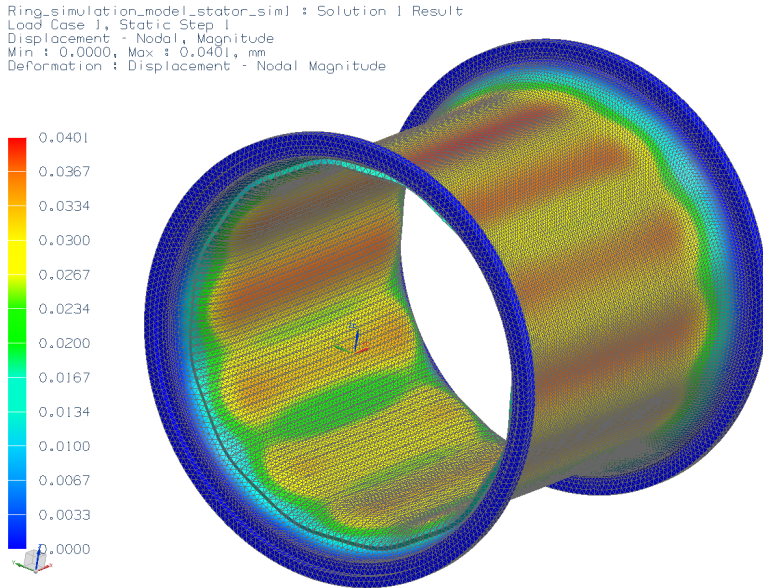


Figure 4.27: Outer stator ring elemental stresses, final simulation LC2



## 4.9 Final simulations



**Figure 4.28:** Outer stator ring displacement, final simulation LC2

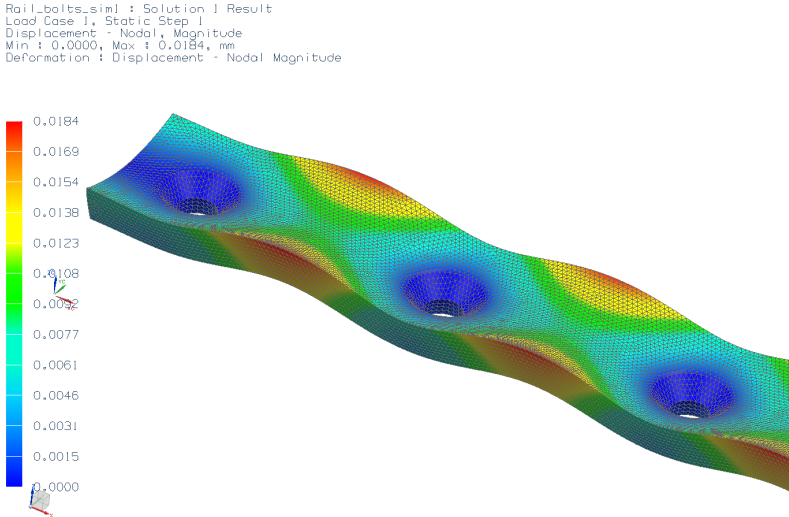
### 4.9.1.6 Rails

Static simulation					
Load case	Number of bolts	Von mises stress elemental [MPa]	Displacement [mm]	Stress amplitude incl. - corr. factors (1.33) [MPa]	Fatigue limit (243MPa) utilization factor
LC5 (SSL = 730mm)	7	112.7	0.018	150.0	150.0/243 = 0.62
LC5 (SSL = 610mm)	7	110.1	0.015	146.4	146.4/243 = 0.60

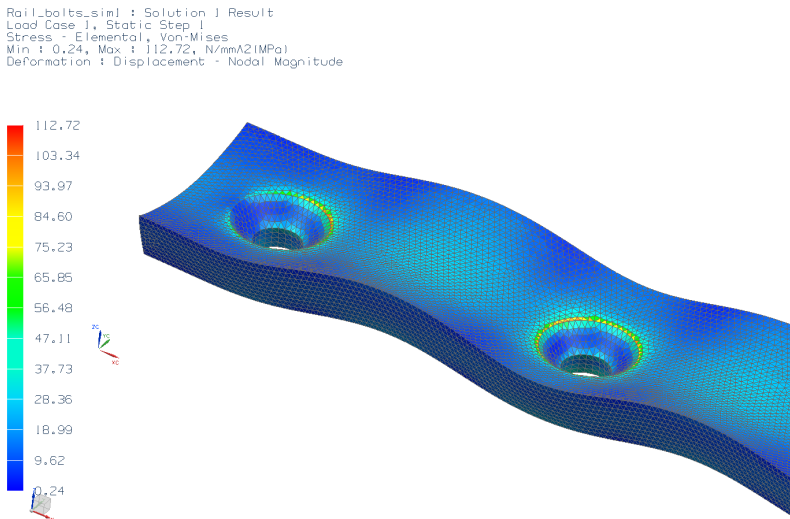
**Table 4.23:** Final simulation result of the rail, LC5

7 bolts were used, and placed with equal distance between each other. The outer holes were placed close to the edge, as this proved to reduce the displacement. The holes were 111mm and 91mm apart (respectively SSL=730mm and 610mm) and the center of the outer holes are 32mm from the edge of the rail. The deformations of the 730mm

long rail are shown in Figure 4.29. The stress values are below the fatigue limit (62% and 60% utilization factor), and the design is approved.



**Figure 4.29:** Deformations on the rail with SSL=730mm



**Figure 4.30:** Elemental stresses on the rail with SSL=730mm

## 4.9.2 ULS results

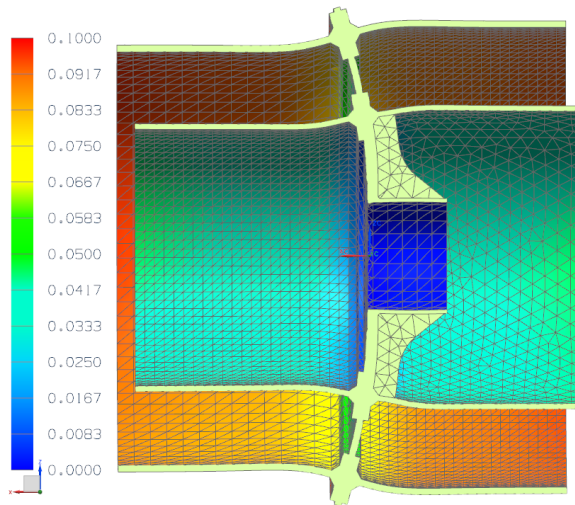
### 4.9.2.1 Rotor structure

Static simulation				
Load case	Von mises stress elemental [MPa]	Displacement [mm]	Stress incl. - safety factor (1.1) [MPa]	Yield stress (190 MPa) utilization factor
LC4	12.1	0.10	13.3	0.07

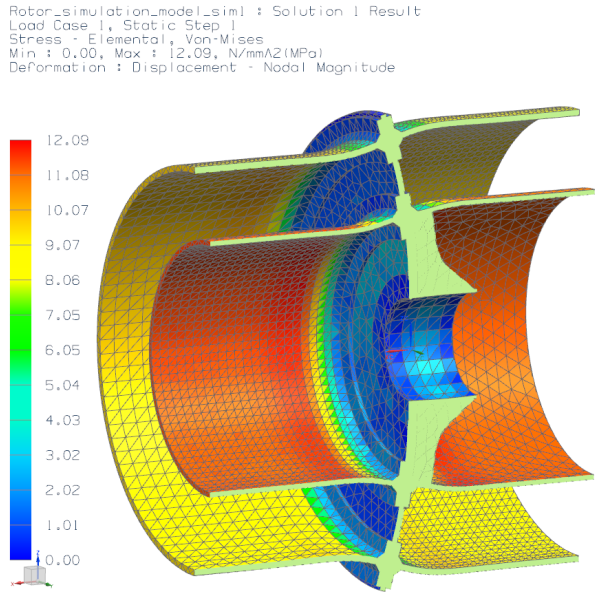
**Table 4.24:** Final results rotor structure assembly

The results from the static simulations of the final rotor structure are shown below. As stated before, this is not a realistic load case which could happen during operation. However, the load case is worse than the actual load case, and the stresses (Figure 4.34) are within the specified limit. The rotor structure design is approved.

Rotor\_simulation\_model\_sim1 : Solution 1 Result  
 Load Case 1, Static Step 1  
 Displacement - Nodal, Magnitude  
 Min : 0.0000, Max : 0.1000, mm  
 Deformation : Displacement - Nodal Magnitude



**Figure 4.31:** Rotor structure displacement



**Figure 4.32:** Rotor structure elemental stresses

**4.9.2.2 Stator structure**

Static simulation				
Load case	Von mises stress elemental [MPa]	Displacement [mm]	Stress incl. - safety factor (1.1) [MPa]	Yield stress (190 MPa) utilization factor
LC4	10.0	0,10	11.0	0.06

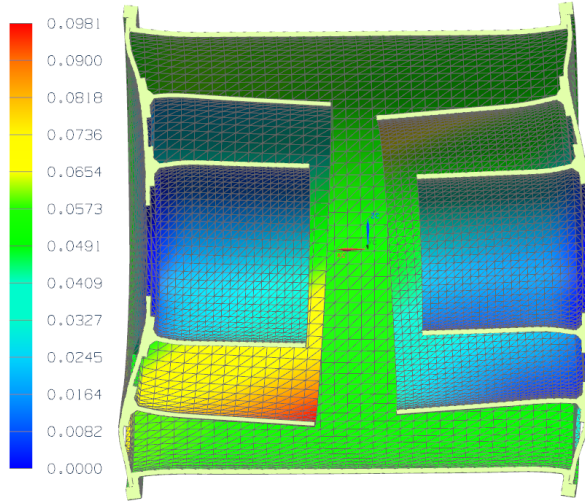
**Table 4.25:** Final results stator structure assembly

The results from the static simulations of the final stator structure are shown below. As for the rotor, this is an unrealistic load case is worse than the actual load case. The stresses (Figure 4.34) are within the specified limit and the stator structure design is approved.

## 4.9 Final simulations

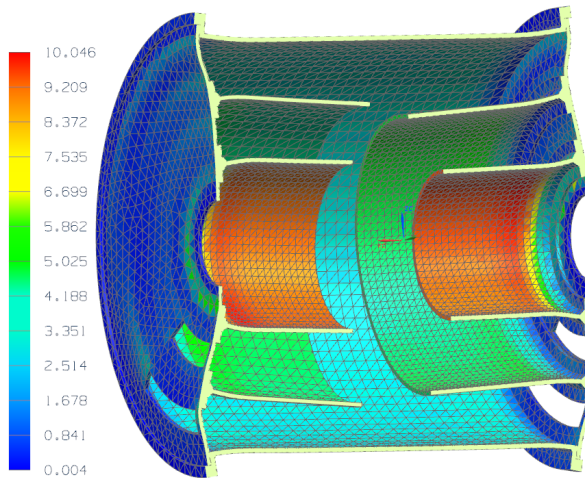
---

Stator\_simulation\_model\_sim1 : Solution 1 Result  
Load Case 1, Static Step 1  
Displacement - Nodal Magnitude  
Min : 0.0000, Max : 0.0981, mm  
Deformation : Displacement - Nodal Magnitude



**Figure 4.33:** Stator structure displacement

Stator\_simulation\_model\_sim1 : Solution 1 Result  
Load Case 1, Static Step 1  
Stress - Elemental, Von-Mises  
Min : 0.004, Max : 10.046, N/mm<sup>2</sup>(MPa)  
Deformation : Displacement - Nodal Magnitude



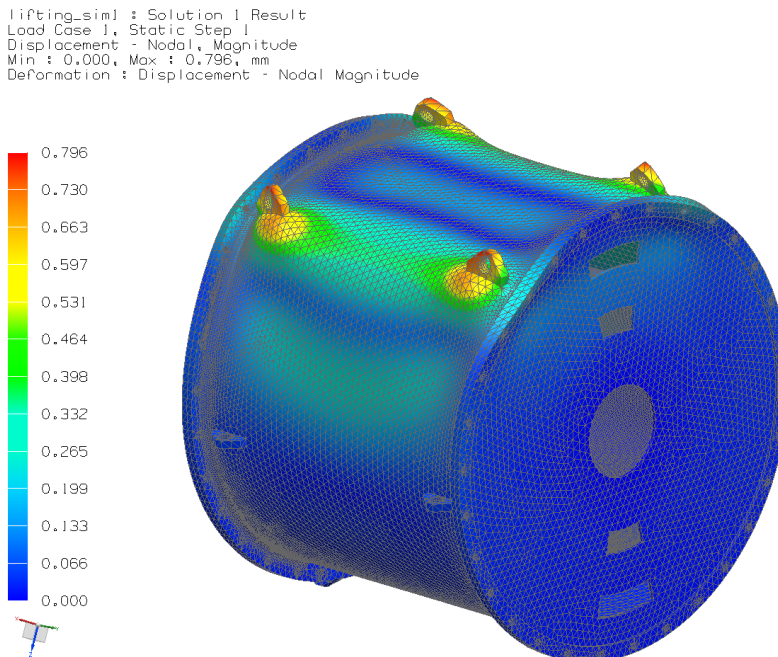
**Figure 4.34:** Stator structure elemental stresses

### 4.9.2.3 Lifting simulation

Static simulation			
Load case	Von mises stress elemental [MPa]	Displacement [mm]	Yield stress (190 MPa) utilization factor
LC6	181.1	0.80 mm	0.95

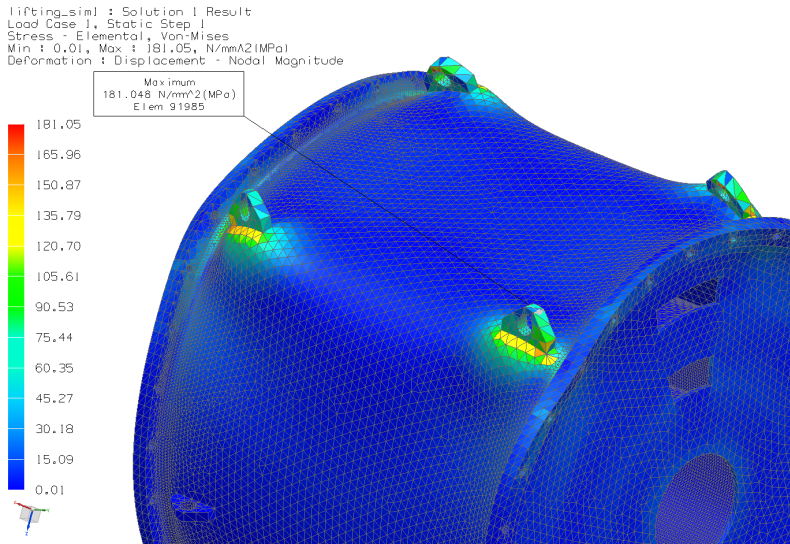
**Table 4.26:** Results, lifting scenario

The displacement of the structure is shown in Figure 4.35 and is approved, as the value is more than six times smaller than the air gap. The peak stresses are located in the transition between the outer stator ring and the lifting points. The total result gives 95% utilization of the ULS stress limit, and the carrying structure is approved. The lifting points will be welded onto the outer stator ring, and these welding areas got the peak stresses. The design of the lifting points will have to be further analyzed, as this simulation mainly tested the carrying structure.



**Figure 4.35:** Displacement from the lifting simulation

## 4.9 Final simulations



**Figure 4.36:** Stresses from the lifting simulation

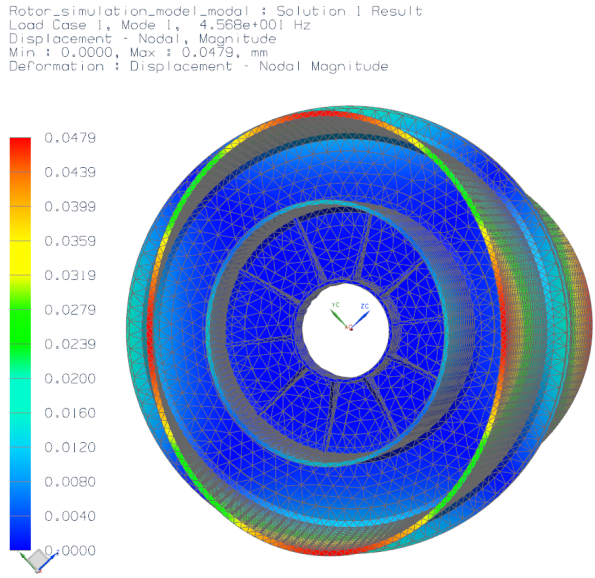
### 4.9.3 ELS results

#### 4.9.3.1 Rotor structure

The lowest eigenfrequency of the rotor structure is 45.7 Hz, which is above the limit specified in subsection 4.5.4. The behavior of the lowest eigenmode is shown in Figure 4.37, where the outer rings are flexing. This eigenmode frequency can be increased by further stiffening of the outer rings and the torque plate.

Eigenmode simulation	
Lowest eigenmode frequency	Eigenmode limit (43.2 Hz) safety factor
45.7 Hz	1.06

**Table 4.27:** Final results rotor structure, eigenmode simulation



**Figure 4.37:** Rotor structure eigenmode simulation final result. Deformation values does not represent real deformations

**4.9.3.2 Stator structure**

The lowest eigenfrequency of the stator structure is 45.7 Hz, which is above the limit specified in subsection 4.5.4. In the mentioned eigenmode, the outer ring moves back and forth axially. Making the torque plates stiffer and reducing the weight of the outer ring can increase the eigenmode frequency.

Eigenmode simulation	
Lowest eigenmode frequency	Eigenmode limit (41.1 Hz) safety factor
45.7 Hz	1.11

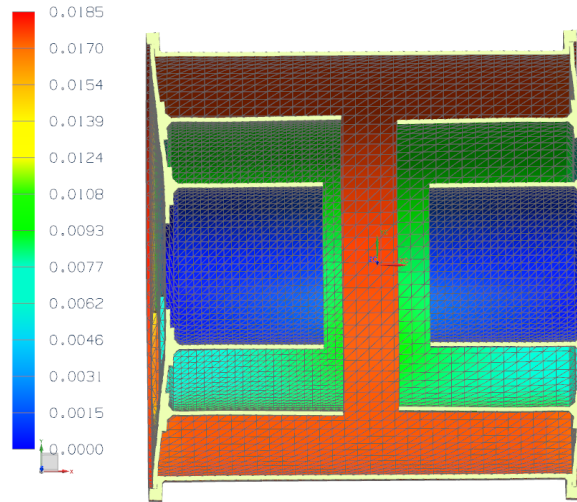
**Table 4.28:** Final results stator structure, eigenmode simulation



## 4.10 Lightweight materials

---

Stator\_simulation\_model\_modal : Solution 1 Result  
Load Case 1, Mode 1, 4.573e+001 Hz  
Displacement - Nodal, Magnitude  
Min : 0.0000, Max : 0.0185, mm  
Deformation : Displacement - Nodal Magnitude



**Figure 4.38:** Stator structure eigenmode simulation final result. Deformation values does not represent real deformations

## 4.10 Lightweight materials

All parts in the current design are made of stainless steel. The weight of the generator is not very important if being used in a tidal turbine application. However, in a windmill application, weight would be of more importance.

Composites would considerably reduce the weight, but also create new challenges. If the rings were made of composites they would be non-conductive, which is beneficial in multiple air gap generators (section 2.2). As composite is a weak material in compression and vulnerable against abrasion, new solutions for the connections between the different components must be developed. Composites are also very sensitive to heat, and loose stiffness as the temperature increases. There have been done some tests with composites for some parts of the SWAY [7] wind turbine generator. In these tests, the use of composites has proved to be unsuccessful mainly due to poor mechanical properties at operational temperatures. In principal concern, due to the poor mechanical properties at increased temperatures, composite as structural material may not be suitable.

If another material is used, the dynamic behavior would be changed. Both the weight and the stiffness of the structure influence the resonance frequency. As the dynamic

simulations in NX are time consuming, some estimations were done by hand.

The spring constant,  $k$ , is derived below:

$$\sigma = \frac{F}{A} = E\varepsilon = E\frac{\Delta l}{l} \rightarrow \frac{EA}{l} = \frac{F}{\Delta l} = k \quad (4.10)$$

The resonance frequency,  $f_r$ , is defined as the square root of the spring constant divided by the mass:

$$f_r = \sqrt{\frac{k}{m}} = \sqrt{\frac{EA}{l\rho V}} \quad (4.11)$$

Equation 4.11 shows that the resonance frequency is dependent of the E-modulus and the density together with the volume which gives the mass of the geometry. For several of the parts of the carrying structure, the eigenmode simulations became the dimension factor. With the same thickness of the parts (equal volume), aluminum will give about the same eigenfrequencies as steel (Equation 4.12):

$$\left(\frac{E_{steel}}{\rho_{steel}} = \frac{207}{7.8} = 26.5\right) \approx \left(\frac{E_{aluminium}}{\rho_{aluminium}} = \frac{70}{2.7} = 25.9\right) \quad (4.12)$$

Aluminum can be used as material for some of the parts with the lowest stress and strain values. No parts will be designed with aluminum as material in this project, but can be an option for optimization at a later stage. Two eigenmode simulations of identical stator structures in both aluminum and steel were done, which verified our estimate:

<b>Stator structure</b>	<b>Steel</b>	<b>Aluminum</b>
Eigenmode:	Frequency [Hz]	
Mode 1:	48.8	49.1
Mode 2:	88.4	88.7
Mode 3:	89.1	89.4
Mode 4:	95.1	94.7

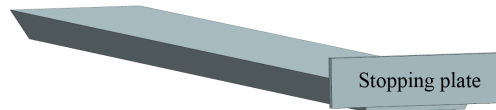
**Table 4.29:** Result from the eigenmode simulations of the stator structure in aluminum and steel

## 4.11 Assembly

The following chapter gives a brief step-by-step description of the generator assembly. Small details such as details in bolt connections and welds will not be given here.

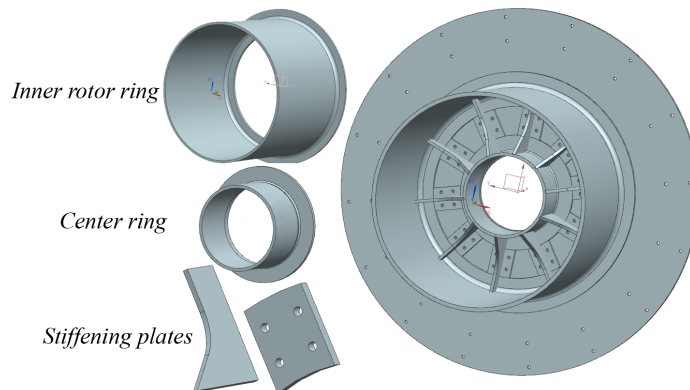
### Rotor preparatory work

1. Stopping plates are welded to the rails



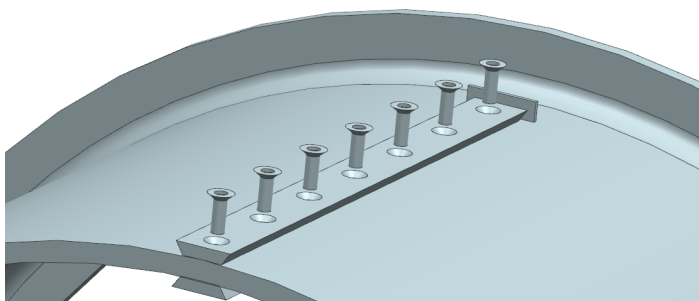
**Figure 4.39:** Welding of stopping plates

2. Inner ring on rotor, stiffening plates and center ring are mounted to the rotor torque plate and spot welded together, then taken off the torque plate for final welding



**Figure 4.40:** Mounting of stiffening parts to the rotor torque plate

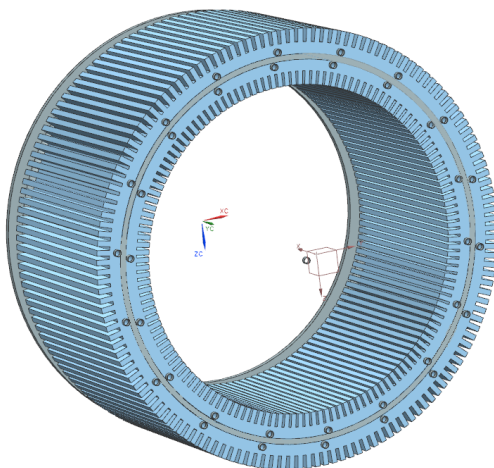
3. Rails are bolted to the rotor rings



**Figure 4.41:** Bolting of rails to ring

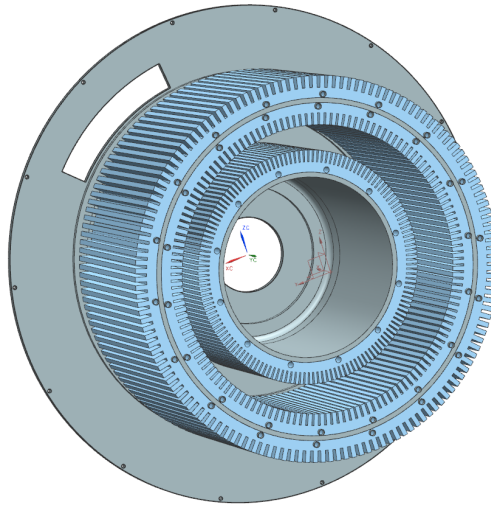
### Stator preparatory work

1. Cooling pipes are placed inside the cooling ducts in the laminations
2. Laminations are shrunk onto the stator rings and the stator outer structure



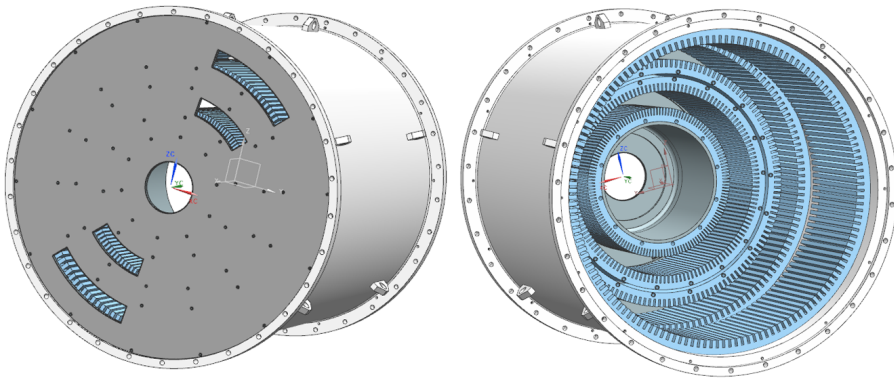
**Figure 4.42:** Laminations shrunk onto the middle stator ring

3. Windings and wiring are installed to the laminations, as well as connecting the cooling system
4. The stator rings are bolted to the stator torque plates



**Figure 4.43:** Bolting of stator rings to torque plate

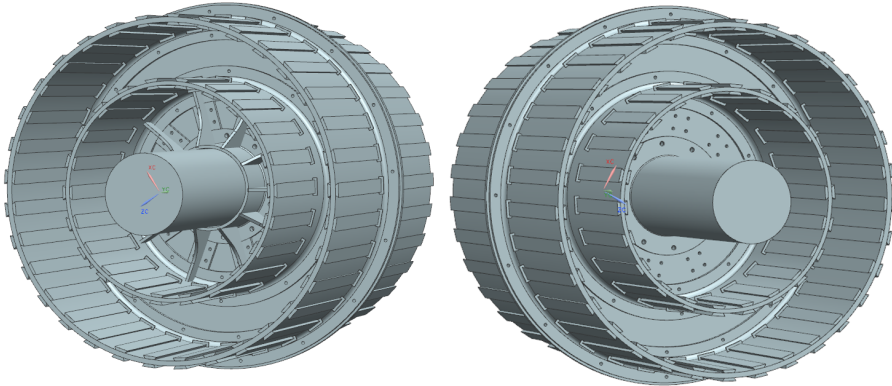
5. One of the torque plates and its rings are bolted to the outer stator structure



**Figure 4.44:** Mounting torque plate and outer stator ring together

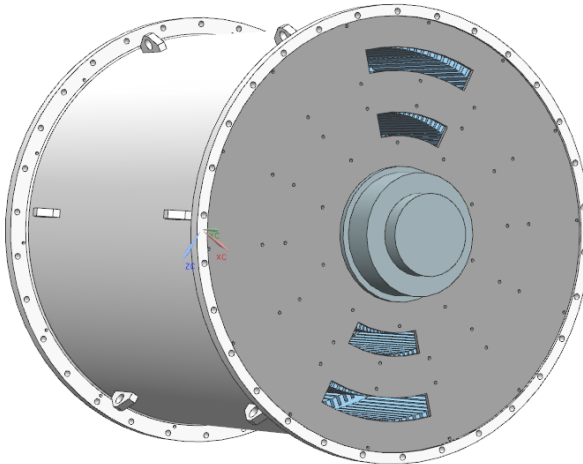
### Assembly

1. The axle is inserted through the rotor torque plate and bolted to one side of the plate. The inner rotor ring and center ring are mounted to the torque plate at the same time, as the axle and the center ring share the same bolts
2. The rest of the rotor rings are bolted to the rotor torque plate



**Figure 4.45:** Rotor torque plate, rings and axle assembly

3. Stator structure is slid onto the rotor and axle. Bearing is mounted/shrunk onto the axle and bolted to the stator torque plate

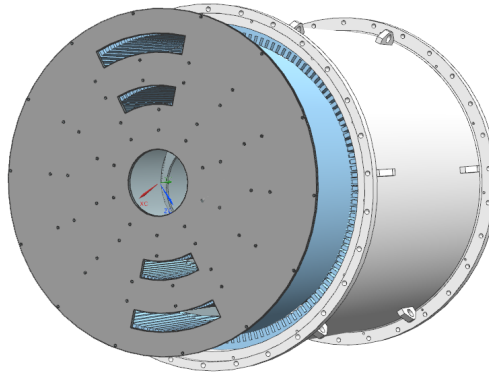


**Figure 4.46:** Stator and rotor structure assembled

4. The other side of the stator (torque plate and rings) are slid onto the rotor and

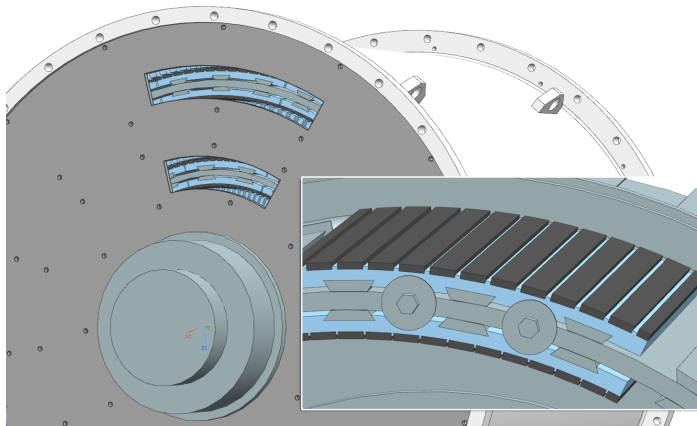
bolted to the stator outer ring

5. Bearing is shrunk onto the axle and bearing housing is bolted to the stator torque plate



**Figure 4.47:** Rotor torque plate and rings are slid into the stator

6. Magnet/lamination segments are inserted onto the rotor rings trough holes in the stator torque plates
7. The segments are locked in place with bolts and washers at the outer edge of the rings



**Figure 4.48:** Insertion of magnet segments





# 5 Conclusion

## 5.1 Results

The goal of this master thesis was to design a carrying structure for a generator using a multi air gap principle. The generator, using SmartMotor's new electromagnetic principle, will generate 1.1 MW. The estimated weight is 25.4 tons. The total dimensions are 2.32m in diameter (excluding bearings) and 2.035m in axial length. The electromagnetic requirements from SmartMotor and the mechanical design limits defined have been fulfilled.

Rings were chosen over beams as carrying structure for the active parts, as they proved to give less displacements. The rings do not only support them self, but helps stiffening the whole structure. To achieve the target 1.1 MW of power output, different generator dimensions were analyzed. Decreasing the diameter and increasing the axial length proved to be the best total solution. The torque plates were the weakest link in the structure, and reducing the diameter gave less displacement.

The dynamic behavior of the parts proved to be the limiting design factor (ELS) for the carrying structure. 1.7 times the frequency of the oscillation forces was used as design limit. Several modifications had to be made to the initial design of the rotor structure. Stiffening plates and a ring were added, and the thickness of the torque plate and outer rotor ring were increased. The stator structure met the design limit without changes to the initial design.

None of the main structural parts had problems with the fatigue design limit (FLS). The stator rings got peak stresses inclusive correction factors of 11 MPa, 3 MPa and 12 MPa, respectively the inner, middle and outer ring. Peak stresses from the rotor ring simulations were 5 MPa and 3 MPa, respectively inner and outer ring. All values were well below the FLS ring stress limit of 131 MPa. The rails are made of a harder material than the rings, which gave the FLS stress limit of 243MPa. Both the rails had peak stresses below this limit included stress correction factors. 113 MPa for the 730mm long rails and 110 MPa for the 610mm long rails.

The ULS stress limit was for the stator and rotor carrying structure, 190 MPa. The lifting simulation was the worst ULS simulation, and a utilization factor of 95% of the ULS limit was achieved.

## 5.2 Discussion

To ease the simulations and save time, some simplifications have been done:

- Forces estimated as sinusoidal curves
- Simplified load case for the rotor and stator structure simulations
- No bolt connections or welding, using unite and fixed constraint instead

The simplifications have reduces the accuracy of the results, but also made the load cases conservative to ensure that all dimensions have been on the safe side.

In a windmill application, the weight would be of more importance. Some quick analysis on aluminum were done, which proved to give about the same eigenfrequencies as steel. Due to the low stresses and strains in the static simulations, aluminum could be used as material for some parts of the carrying structure. Composites would also reduce the weight, but is challenging to use due to poor mechanical properties at increased temperatures.

The main focus in this thesis has been the carrying structure, and further work on the following subjects will be necessary:

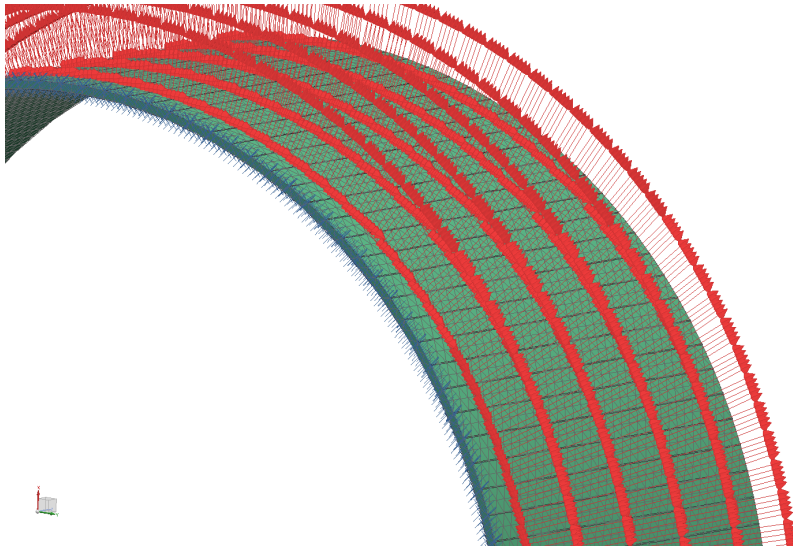
- Selection and analysis of bolt types, class and pretension
- Analysis on the welded joints
- Calculations on needed cooling
- Selection of axle design and type of bearings

## 6 Appendix A - Simulation ring vs beams

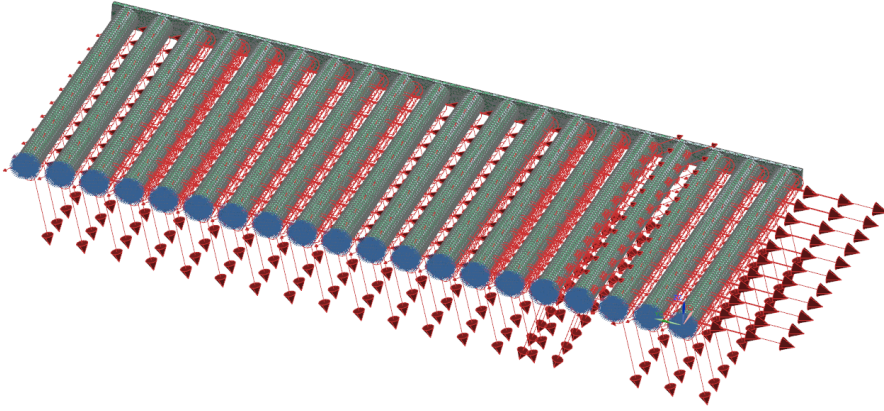
The settings for the simulations in NX are shown below:

- Solution type: SESTATIC 101 - single constraint
- Mesh type: CTETRA(10)
- Mesh size:
  - Rings: 30mm
  - Beams: 15mm
- Material: Steel ( $E = 207 \text{ GPa}$ )

Fixed constraint was used and can be seen as the blue indicators on the ring and beam edges in (Figure 6.1) and (Figure 6.2). The simulations were performed on a complete ring, 132 forces. In the beam simulation, one beam was used for each magnet. A thin ring was used to connect the ends of the beams. 20 beams were used to reduce the amount of work.



**Figure 6.1:** Simulation setup of the ring



**Figure 6.2:** Simulation setup of the beams

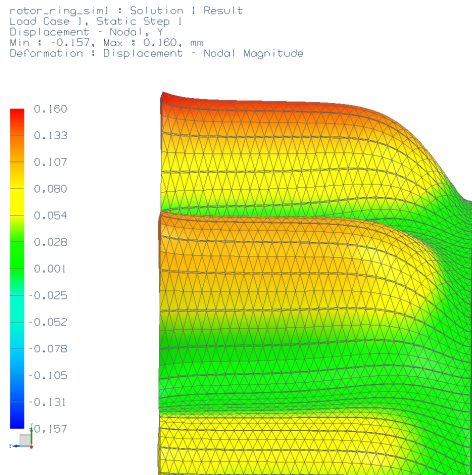
Results ring simulations				
Diameter	Axial lenght	Thickness	Radial displacement	Max stress elemental
2590 mm	350 mm	20 mm	0.153 mm	20.2 MPa
2590 mm	400 mm	20 mm	0.155 mm	20.6 MPa
2590 mm	500 mm	20 mm	0.157 mm	23.9 MPa
2590 mm	1000 mm	20 mm	0.160 mm	24.4 MPa

**Table 6.1:** Results from the simulations on rings, with radial and tangential forces

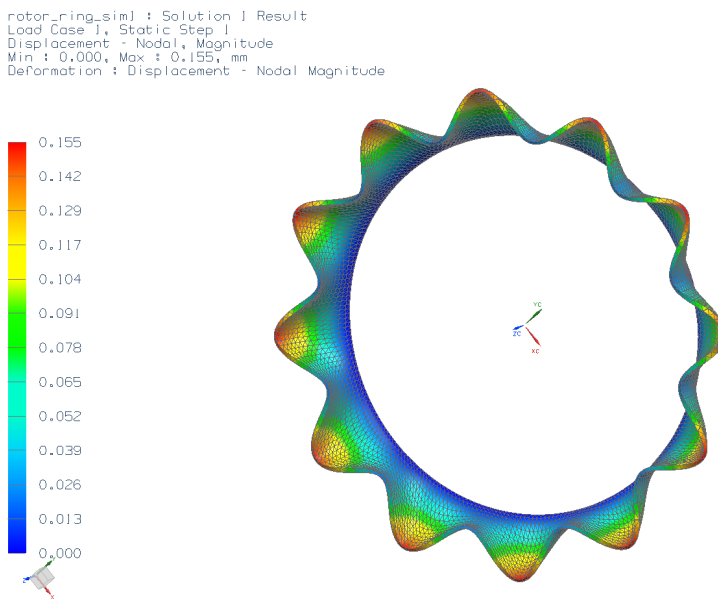
Results beam simulations			
Axial lenght	Thickness	Radial displacement	max stress elemental
350 mm	40 mm	0.938 mm	144 MPa
400 mm	40 mm	1.58 mm	180 MPa
500 mm	40 mm	3.78 mm	262 MPa

**Table 6.2:** Results from the simulations on beams, with radial and tangential forces

The simulations shows a significant difference in displacement in the radial direction between the two principles. Even though the rings axial length increases, both the stresses and the displacement are about the same. The ring stretches only to a certain limit (Figure 6.3), even though the axial length increases. The beams suffer from larger displacements and stresses than the rings, and the difference increases as the axial length of the beam increases.

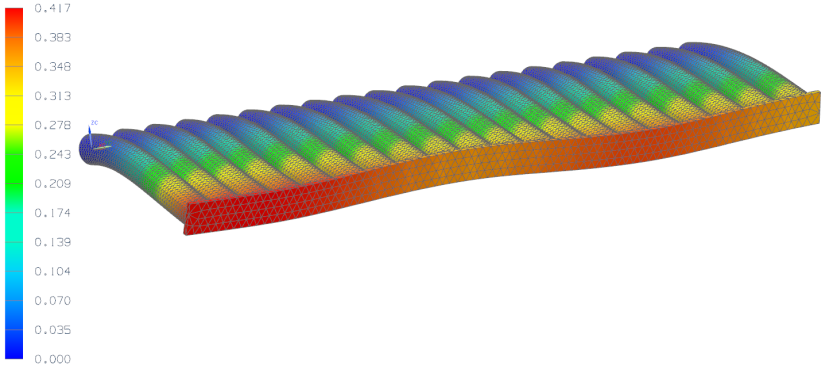


**Figure 6.3:** Ring with axial length of 1000mm, displacements



**Figure 6.4:** Radial displacement, ring with 400mm axial length

beams\_test\_connected\_sim1 : Solution 1 Result  
Load Case 1, Static Step 1  
Displacement - Nodal, Magnitude  
Min : 0.000, Max : 0.417, mm  
Deformation : Displacement - Nodal Magnitude



**Figure 6.5:** Radial displacement, segment of beams connected with a thin ring. Axial beam length of 400mm

# 7 Appendix B - Preliminary simulations results

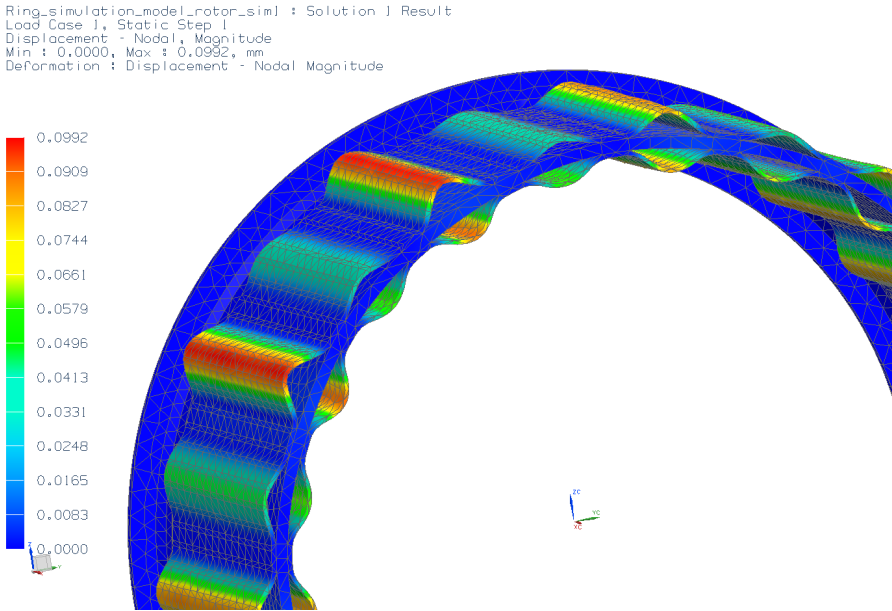
## 7.1 Static ring simulations

Rings from three different generator geometries with the same power output; 1.1 MW, were tested in these simulations. The axial length of the active area on the rings were changed between the following lengths: 300 mm, 500 mm and 700 mm. Results for the rotor rings are shown in Table 7.1 and the stator ring results are shown in Table 7.2.

Rotor rings						
Load case	Weight [N]	SSL [mm]	Diameter [mm]	Number of rails	Displacement [mm]	Stress ele. [MPa]
LC1	10600	300	1965	22	0.13	39.9
LC1	14100	300	2580	22	1.18	78.5
LC1	11900	500	1465	22	0.037	28.5
LC1	17200	500	2080	22	0.15	42.2
LC1	12900	700	1195	22	0.015	7.3
LC1	20000	700	1810	22	0.099	38.6
LC1	16400	700	1500	22	0.0315	25.4
LC1	16400	700	1500	33	0.00632	7.14

**Table 7.1:** Results from the preliminary rotor ring simulations

On the rotor rings the laminations proved to be the biggest contributor to the total displacement, see Figure 7.1 for illustration. The laminations get pulled outwards while the ring suffers from very small deformations. Rings with large diameters got higher deflections due to increased distance between the rails. A test with increased number of rails was performed on a ring with SSL of 700mm and a diameter of 1500. With 33 rails compared to 22, the deflections were reduced from 0.0315mm to 0.00632mm. The simulations show that all the rotor rings have small deformations.



**Figure 7.1:** Rotor ring deformations. 22 rails, axial length 700mm and diameter of 1810 mm

Stator rings						
	Load case	Weight [N]	SSL [mm]	Diameter [mm]	Displacement [mm]	Stress ele. [MPa]
Inner rings	LC2	10700	300	1569	0.0174	5.5
	LC2	11100	500	1069	0.010	5.6
	LC2	11100	700	799	0.0094	5.3
Middle ring	LC1	24900	300	2189	0.0045	1.5
	LC1	29900	500	1689	0.0035	1.3
	LC1	35296	700	1419	0.0042	1.4
Outer ring	LC3	29600	300	2760	0.049	9.1
	LC3	30300	500	2260	0.037	8.2
	LC3	32600	700	1990	0.033	8.2
	LC2	29600	300	2760	0.050	9.8
	LC2	30300	500	2260	0.037	8.7
	LC2	32600	700	1990	0.032	8.5

**Table 7.2:** Results from the preliminary stator ring simulations

On the stator rings the laminations are shrinked onto the rings, and mesh mating used on the adjoining faces. Due to this there are no relative movement between laminations and ring (Figure 7.2). Overall, the displacements of the rings were low and in the range

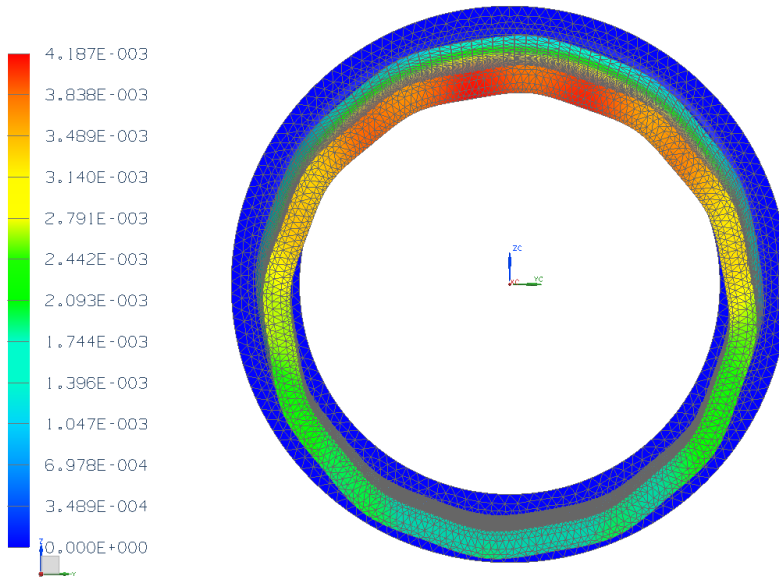


## 7.2 Static rotor structure simulations

---

from 0.0035mm to 0.050mm. The stresses are as the deflections low, varying between 1.3 MPa and 9.8 MPa.

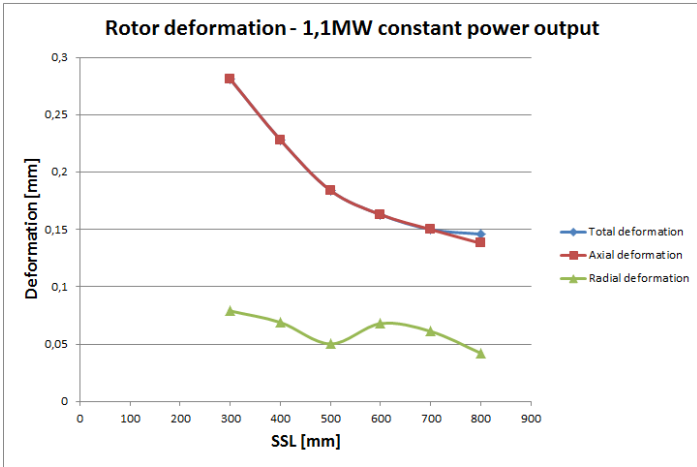
```
Ring_simulation_model_stator_sim1 : Solution 1 Result  
Load Case 1, Static Step 1  
Displacement - Nodal, Magnitude  
Min : 0.000E+000, Max : 4.187E-003, mm  
Deformation : Displacement - Nodal Magnitude
```



**Figure 7.2:** Stator middle ring deformations, axial length 700mm and diameter of 1419mm

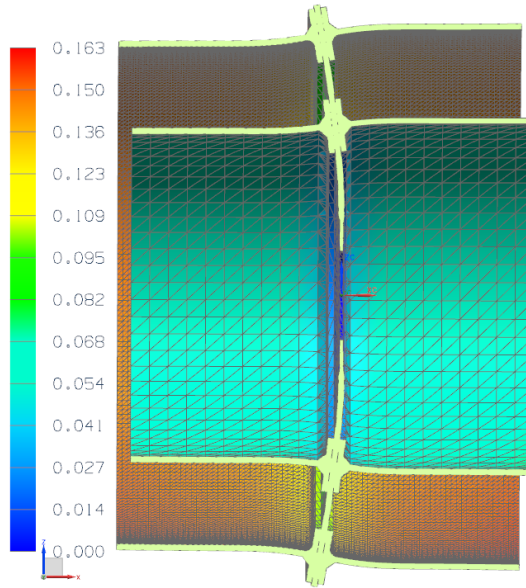
## 7.2 Static rotor structure simulations

The rotor was tested with several different dimensions and all with load case LC4. The power output target of 1.1MW was kept constant, which meant that increasing the ring lengths would reduce the total diameter of the generator. The results show that increasing the length of the generator decreases the deformations (Figure 7.3), as a larger torque plate does not deflect as much as a smaller one. The radial deformations of the rings will only deform to a certain level, as shown in ring the simulations, Table 7.1 and Table 7.2. In fact the axial deformations are 2-4 times larger than the radial deformations.



**Figure 7.3:** Rotor deformations, simplified simulations

Rotor\_simulation\_model\_sim1 : Solution 1 Result  
Load Case 1, Static Step 1  
Displacement - Nodal, Magnitude  
Min : 0.000, Max : 0.163, mm  
Deformation : Displacement - Nodal Magnitude



**Figure 7.4:** Magnitude of deformations for rotor, SSL=0,6m

## 7.3 Static stator structure simulations

As with the rotor, the stator was tested with different diameters while keeping the 1.1MW power output goal constant. The results are shown in Figure 7.5. The deformations decrease slightly when the length of the rings is increased. Axial deformations are larger than radial deformations, but the difference decreases with the length of the rings. This is because the weight of the rings and the active parts increases for longer rings. This effect can be seen in Figure 7.6.

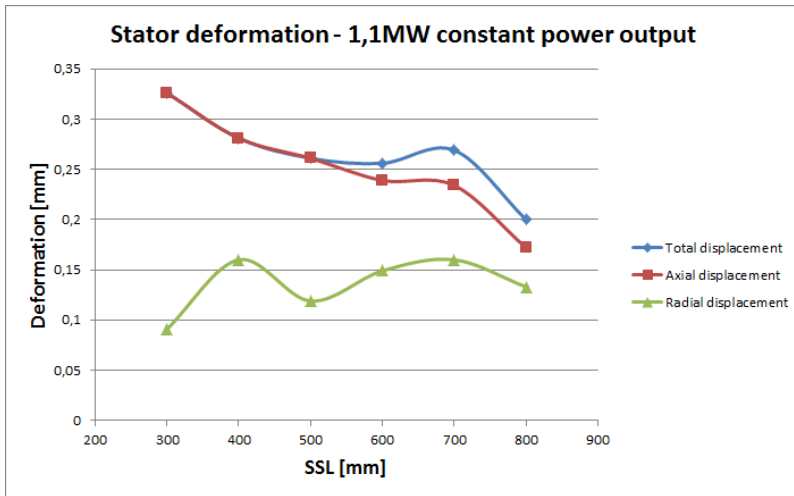
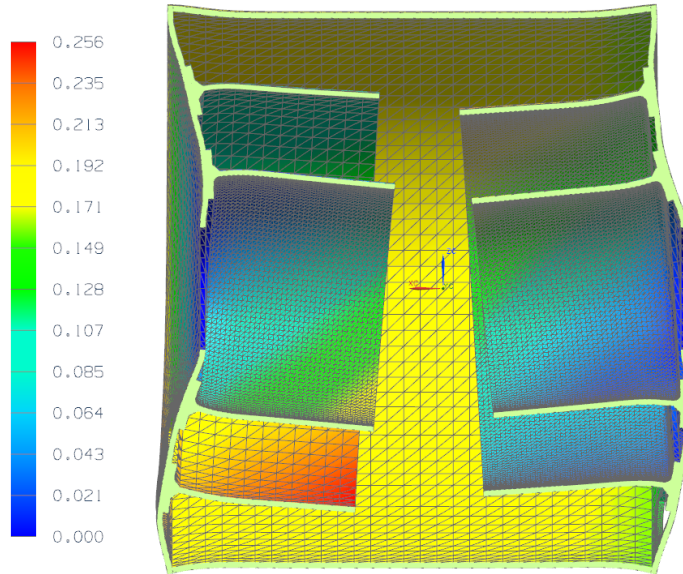


Figure 7.5: Stator deformations, simplified simulations

```

Stator_simulation_model_sim1 : Solution 1 Result
Load Case 1, Static Step 1
Displacement - Nodal, Magnitude
Min : 0.000, Max : 0.256, mm
Deformation : Displacement - Nodal Magnitude

```



**Figure 7.6:** Magnitude of deformations for stator, SSL=0,6m

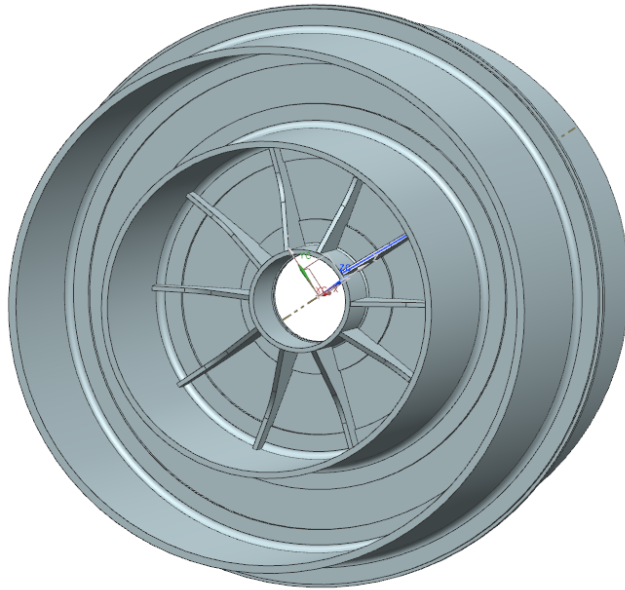
## 7.4 Eigenmode simulations

### 7.4.1 Rotor

Initial simulations with the exact same shape and dimensions as in subsection 4.7.2.1 had two eigenmodes with a frequency of 24 Hz and two modes with 44 Hz. The problem was that the torque plate was flexing too much. This also meant that increasing the diameter lowered the eigenfrequencies (another proof that smaller diameter is beneficial).

In order to achieve the lower frequency limit, 10 stiffening plates were added to the inside of the inner rotor ring (only on one side of the torque plate as the axle mounts to the outer side). A small diameter ring was added close to the center of the torque plate, which allowed for a larger fastening area for the stiffening plates (Figure 7.7).

The length of the inner rotor rings were decreased to make room for the stiffening plates, and the outer rings in turn increased (to maintain the required power output). These changes, combined with a 25 mm (+5 mm) thick torque plate and 25 mm (+5



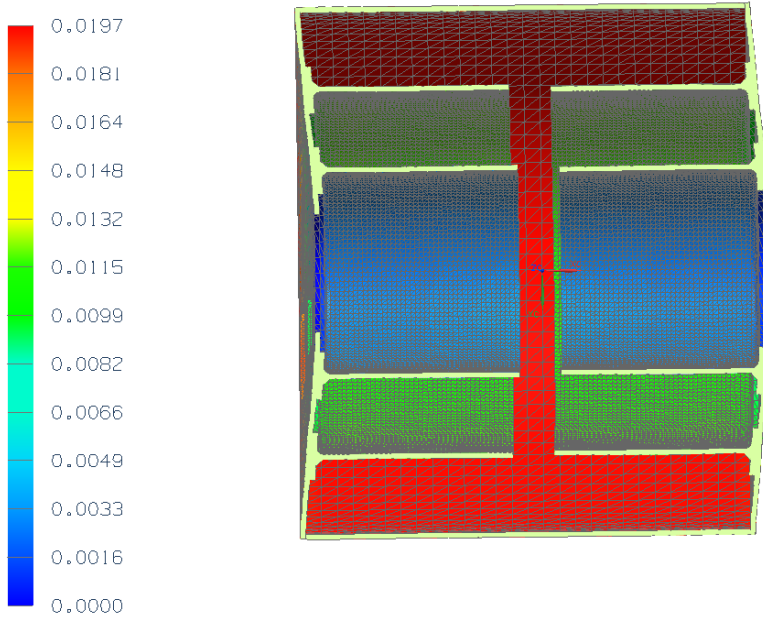
**Figure 7.7:** Stiffening plates and ring, rotor structure

mm) outer ring thickness, increased the lowest eigenfrequency to 46,7 Hz. Increasing the eigenfrequencies further required substantial changes to the structure, making production and assembly more difficult and expensive.

### 7.4.2 Stator

The first eigenmode simulation for the stator was done with the exact same dimensions as on the last static simulations (subsubsection 4.7.2.2). The lowest eigenmodes from this simulation had a frequency of 48.8 Hz, and the next eigenmode frequency was 88.4 Hz. The lowest eigenmode had deformations of the torque plate, making the outer ring move back and forth axially. The result was approved, and no dimensions were changed besides small changes to the length of the rings and additional outer ring flanges.

Stator\_simulation\_model1 : Solution 1 Result  
Load Case 1, Mode 1, 4.878e+001 Hz  
Displacement - Nodal, Magnitude  
Min : 0.0000, Max : 0.0197, mm  
Deformation : Displacement - Nodal Magnitude



**Figure 7.8:** Deformations from eigenmode simulations on the stator



## 8 Appendix C - Material

### Stainless steel, austenitic, AISI 304L, wrought

#### General properties

##### Designation

AISI 304L

UNS number

S30403

Density

7.8e3 - 8.01e3 kg/m<sup>3</sup>

Price

\* 37.5 - 41.2 NOK/kg

##### Tradenames

ARGESTE 4306 LA/LF/SB/VC, Stahlwerk Ergste Westig GmbH (GERMANY); STAINWELD 308-15, Lincoln Electric Co. (USA); STAINWELD 308-16, Lincoln Electric Co. (USA); SPARTAN REDHEUGH 305S19, Spartan Redheugh Ltd (UK); EASTERN STAINLESS TYPE 347, Eastern Stainless Corp. (USA); PROJECT 70 STAINLESS TYPE 347, Carpenter Technology Corp. (USA); EASTERN STAINLESS TYPE 304L, Eastern Stainless Corp. (USA); PROJECT 7000 STAINLESS TYPE 304L, Carpenter Technology Corp. (USA); PROJECT 70 STAINLESS TYPE 304L, Carpenter Technology Corp. (USA); SPARTAN REDHEUGH 347S31, Spartan Redheugh Ltd (UK); ARGESTE 3956 AN, Stahlwerk Ergste Westig GmbH (GERMANY); EASTERN STAINLESS TYPE 321, Eastern Stainless Corp. (USA); PROJECT 70 STAINLESS TYPE 321, Carpenter Technology Corp. (USA); ARGESTE 4541 TA/SC/TB/TW, Stahlwerk Ergste Westig GmbH (GERMANY); SPARTAN REDHEUGH 321S31, Spartan Redheugh Ltd (UK);

#### Composition overview

##### Composition (summary)

Fe/&lt;.03C/17.5-19Cr/9-12Ni/.5-2Mn/.2-1Si/&lt;.045P/&lt;.03S

Base

Fe (Iron)

##### Composition detail

C (carbon)	0	-	0.03	%
Cr (chromium)	17.5	-	19	%
Fe (iron)	65.9	-	72.8	%
Mn (manganese)	0.5	-	2	%
Ni (nickel)	9	-	12	%
P (phosphorus)	0	-	0.045	%
S (sulfur)	0	-	0.03	%
Si (silicon)	0.2	-	1	%

##### Bio-data

RoHS (EU) compliant grades?

True

Toxicity rating

Non-toxic

Food contact grades? (FDA, EU, BfR, NSF)

False

#### Mechanical properties

Young's modulus	191	-	205	GPa
Flexural modulus	* 191	-	205	GPa
Shear modulus	74	-	82	GPa
Bulk modulus	135	-	152	GPa
Poisson's ratio	0.265	-	0.275	
Shape factor	63			
Yield strength (elastic limit)	190	-	310	MPa
Tensile strength	480	-	620	MPa
Compressive strength	* 190	-	310	MPa
Flexural strength (modulus of rupture)	190	-	310	MPa
Elongation	* 45	-	60	% strain
Hardness - Vickers	* 170	-	210	HV
Hardness - Rockwell B	75	-	83	
Hardness - Rockwell C	* 0	-	13.4	
Hardness - Brinell	* 143	-	201	MPa
Fatigue strength at 10 <sup>7</sup> cycles	* 262	-	290	MPa
Fatigue strength model (stress range)	* 150	-	220	MPa
Parameters: Stress Ratio=0, Number of Cycles = 1e7				
Fracture toughness	* 54	-	70	MPa.m <sup>0.5</sup>



Mechanical loss coefficient (tan delta)	* 9.5e-4	-	0.0014	
<b>Thermal properties</b>				
Melting point	1.4e3	-	1.45e3	°C
Maximum service temperature	750	-	925	°C
Minimum service temperature	-273			°C
Thermal conductivity	14	-	16	W/m.°C
Specific heat capacity	490	-	530	J/kg.°C
Thermal expansion coefficient	16	-	18	µstrain/°C
Latent heat of fusion	* 260	-	285	kJ/kg
<b>Processing properties</b>				
Cold forming	Good			
Hot forming	Good			
Machinability - speed	85	-	100	sfm
Weldability - MIG	Excellent			
Weldability - plasma	Excellent			
Weldability - SAW	Excellent			
Weldability - TIG	Excellent			
Carbon equivalency	4.22	-	5.1	
Brazeability	Fair			
<b>Electrical properties</b>				
Electrical resistivity	65	-	77	µohm.cm
<b>Magnetic properties (ambient temperature)</b>				
Ferromagnetic?	False			
<b>Optical properties</b>				
Transparency	Opaque			
<b>Durability: flammability</b>				
Flammability	Non-flammable			
<b>Durability: fluids and sunlight</b>				
Water (fresh)	Excellent			
Water (salt)	Excellent			
Weak acids	Excellent			
Strong acids	Excellent			
Weak alkalis	Excellent			
Strong alkalis	Excellent			
Organic solvents	Excellent			
UV radiation (sunlight)	Excellent			
Oxidation at 500C	Excellent			
<b>Corrosion resistance (relative to other metals)</b>				
Pitting resistance equivalent number (PREN)	17.5	-	19	
Pitting and crevice corrosion	Low (<20)			
Stress corrosion cracking	Moderate			
Intergranular (weld line) corrosion	Good			
Inorganic acids	Moderate			
Organic acids	Moderate			
Alkalis	Moderate			
Humidity / water	Excellent			
Sea water	Moderate			
Sour oil and gas	Moderate			

## Stainless steel, austenitic, AISI 304, wrought, 1/4 hard

### General properties

#### Designation

AISI 304

UNS number

S30400

Density

7.85e3 - 8.06e3 kg/m<sup>3</sup>

Price

\* 36.3 - 39.9 NOK/kg

#### Tradenames

RDN 260, Roldan S.A. (SPAIN); RDN 240, Roldan S.A. (SPAIN); RDN 210, Roldan S.A. (SPAIN); RDN 340, Roldan S.A. (SPAIN); YOONSTEEL S2, Yoonsteel (Malaysia) Sdn. Bhd (MALAYSIA); ARGESTE 4306 LA/LF/SB/VC, Stahlwerk Ergste Westig GmbH (GERMANY); STAINWELD 308-15, Lincoln Electric Co. (USA); STAINWELD 308-16, Lincoln Electric Co. (USA); EASTERN STAINLESS TYPE 347, Eastern Stainless Corp. (USA); PROJECT 70 STAINLESS TYPE 347, Carpenter Technology Corp. (USA); EASTERN STAINLESS TYPE 304L, Eastern Stainless Corp. (USA); PROJECT 7000 STAINLESS TYPE 304L, Carpenter Technology Corp. (USA); PROJECT 70 STAINLESS TYPE 304L, Carpenter Technology Corp. (USA); SPARTAN REDHEUGH 347S31, Spartan Redheugh Ltd (UK);

### Composition overview

#### Composition (summary)

Fe/&lt;.08C/17.5-20Cr/8-11Ni/&lt;2Mn/&lt;1Si/&lt;.045P/&lt;.03S

Base

Fe (Iron)

#### Composition detail

C (carbon)	0	- 0.08	%
Cr (chromium)	17.5	- 20	%
Fe (iron)	65.8	- 74.5	%
Mn (manganese)	0	- 2	%
Ni (nickel)	8	- 11	%
P (phosphorus)	0	- 0.045	%
S (sulfur)	0	- 0.03	%
Si (silicon)	0	- 1	%

#### Bio-data

RoHS (EU) compliant grades?

True

Toxicity rating

Non-toxic

Food contact grades? (FDA, EU, BfR, NSF)

True

### Mechanical properties

Young's modulus	190	- 203	GPa
Flexural modulus	* 190	- 203	GPa
Shear modulus	74	- 81	GPa
Bulk modulus	134	- 151	GPa
Poisson's ratio	0.265	- 0.275	
Shape factor	39		
Yield strength (elastic limit)	515	- 690	MPa
Tensile strength	860	- 1.03e3	MPa
Compressive strength	* 515	- 690	MPa
Flexural strength (modulus of rupture)	515	- 690	MPa
Elongation	* 10	- 30	% strain
Hardness - Vickers	* 265	- 355	HV
Hardness - Rockwell B	* 102	- 109	
Hardness - Rockwell C	* 25	- 36	
Hardness - Brinell	* 253	- 336	MPa
Fatigue strength at 10 <sup>7</sup> cycles	* 385	- 437	MPa
Fatigue strength model (stress range)	* 243	- 334	MPa
Parameters: Stress Ratio = 0, Number of Cycles = 1e7			
Fracture toughness	* 80	- 137	MPa.m <sup>0.5</sup>
Mechanical loss coefficient (tan delta)	* 4.9e-4	- 6.4e-4	

### Thermal properties

## Appendix C - Material

---

Melting point	1.4e3	-	1.45e3	°C
Maximum service temperature	750	-	925	°C
Minimum service temperature	-273			°C
Thermal conductivity	14	-	17	W/m.°C
Specific heat capacity	490	-	530	J/kg.°C
Thermal expansion coefficient	16	-	18	µstrain/°C
Latent heat of fusion	* 260	-	285	kJ/kg
<b>Processing properties</b>				
Cold forming	Good			
Hot forming	Good			
Machinability - speed	85	-	100	sfm
Weldability - MIG	Excellent			
Weldability - plasma	Excellent			
Weldability - SAW	Excellent			
Weldability - TIG	Excellent			
Carbon equivalency	4.03	-	5.23	
Brazeability	Fair			
<b>Electrical properties</b>				
Electrical resistivity	65	-	77	µhm.cm
<b>Magnetic properties (ambient temperature)</b>				
Ferromagnetic?	False			
<b>Optical properties</b>				
Transparency	Opaque			
<b>Durability: flammability</b>				
Flammability	Non-flammable			
<b>Durability: fluids and sunlight</b>				
Water (fresh)	Excellent			
Water (salt)	Excellent			
Weak acids	Excellent			
Strong acids	Acceptable			
Weak alkalis	Excellent			
Strong alkalis	Excellent			
Organic solvents	Excellent			
UV radiation (sunlight)	Excellent			
Oxidation at 500C	Excellent			
<b>Corrosion resistance (relative to other metals)</b>				
Pitting resistance equivalent number (PREN)	17.5	-	20	
Pitting and crevice corrosion	Low (<20)			
Stress corrosion cracking	Moderate			
Intergranular (weld line) corrosion	Restricted			
Inorganic acids	Moderate			
Organic acids	Moderate			
Alkalis	Moderate			
Humidity / water	Excellent			
Sea water	Moderate			
Sour oil and gas	Moderate			



## 9 Appendix D - Fatigue calculations

Material fatigue values were taken from CES Edupack 2011 [3]. The highest force frequency is found on the rotor rings, and is 26.4 Hz. At  $10^7$  cycles, the running time for the generator is 116 days.  $N = 10^7$  cycles is normally referred to as the fatigue limit. The lifetime of the generator will be more than this, so the  $N = 10^7$  is used in the following calculations.

### 9.1 Calculation of effective stress notch amplitude

From EN 13445-6:2009 [6], the effective notch stress range,  $\Delta\sigma^*$ , is calculated according to the following formula:

$$\Delta\sigma^* = K_{eff} \cdot \frac{\Delta\sigma_{eq,struct}}{f_s \cdot f_e \cdot f_t \cdot f_m} \quad (9.1)$$

where

$\Delta\sigma_{eq,struct}$  = structural stress range

$f_s$  = surface finish correction factor

$f_e$  = wall thickness correction factor

$f_t$  = temperature correction factor

$f_m$  = mean stress correction factor

Modifying the formula for use with effective notch stress amplitude,  $\sigma^*$ , gives the following formula:

$$\sigma^* = K_{eff} \cdot \frac{\sigma_{eq,struct}}{f_s \cdot f_e \cdot f_t \cdot f_m} \quad (9.2)$$

where

$\sigma_{eq,struct}$  = structural stress amplitude

By using  $\gamma_m$  and  $\gamma_n$  from IEC61400 (IEC international standards regarding wind turbines, [4]) instead of  $K_{\text{eff}}$ , we get the modified formula for effective notch stress range:

$$\Delta\sigma^* = \gamma_m \cdot \gamma_n \cdot \frac{\Delta\sigma_{eq,struct}}{f_s \cdot f_e \cdot f_t \cdot f_m} = S_f \cdot \Delta\sigma_{eq,struct} \quad (9.3)$$

and

$$\sigma^* = \gamma_m \cdot \gamma_n \cdot \frac{\sigma_{eq,struct}}{f_s \cdot f_e \cdot f_t \cdot f_m} = S_f \cdot \sigma_{eq,struct} \quad (9.4)$$

where

$\gamma_m$  = partial material correction factor

$\gamma_n$  = consequence of failure correction factor

$S_f$  = Total fatigue safety correction factor

## 9.2 Calculation of surface finish factor $f_s$

For number of cycles above  $2 \cdot 10^6$  ( $N = 10^7$  in this case), the surface finish factor is according to EN 13445-6:2009

$$f_s = 1 - 0,03 \cdot \ln(R_z) \cdot \ln\left(\frac{R_m}{200}\right) \quad (9.5)$$

where

$R_z$  = peak-to-valley height of the material surface

$R_m$  = Tensile strength

$R_z$  is specified as  $50\mu m$  for machined surfaces in clause 18 of EN 13445-3. For rolled surfaces,  $R_z = 200$ . The surface finish factor then becomes:

Material	$R_m$	$R_z$	$f_s$
AISI 304L, machined	480	50	$0,897 \approx 0,90$
AISI 304L, rolled	480	200	$0,861 \approx 0,86$
AISI 304 1/4 hard, machined	860	50	$0,829 \approx 0,83$

**Table 9.1:** Surface finish factor

### 9.2.1 Calculation of wall thickness correction factor

According to EN 13445-6:2009, wall thickness influences the safety factor with the following formula:

$$f_e = F_e^{(0,11nN-0,0465)} \quad (9.6)$$

where

$$F_e = \left( \frac{25}{e_{max}} \right)^{0,182} \quad (9.7)$$

and

$e_{max}$  = maximum wall thickness

For  $e_{max} \leq 25\text{mm}$ ,  $f_e = 1$ .

The rings, stator and rotor structure have a maximum thickness of 20-25mm, and thus  $f_e = 1$ . The stator have outer flanges for mounting the generator to the turbine structure with a thickness up to 60mm, but these flanges will not have high stresses with the simulated load cases.

## 9.3 Calculation of temperature correction factor

The temperature is estimated by SmartMotor to vary between a range of 20-40°C. According to EN 13445-6:2009, this gives  $f_t = 1$  (even for a temperature range of 0-100°C).

## 9.4 Calculation of mean stress correction factor

The rings are assumed to get equally large compressive forces as tensile forces ( $R = -1$ ), meaning the mean stress correction factor  $f_m = 1$ . By assuming the stresses have  $R = 0$  for the rails (which is conservative), the fatigue stress range from CES EduPack at  $R = 0$  can be used. This range has the mean stress correction factor taken into account, thereby  $f_m = 1$  for the rails.

## 9.5 Partial material factor

According to IEC 61400-4, the partial material factor for cast iron fatigue,  $\gamma_m = 1.1$ . The chosen materials for the generator are stainless steel, and are assumed to be of equal or better quality than cast iron.

## 9.6 Consequence of failure factor

The consequence of failure factor  $\gamma_n = 1.0$ , as stated in subsection 4.5.1.



## **10 Appendix E - Weight estimations of the final generator parts**

The total weight (rotor and stator) of the active parts for an air gap of 2665.5mm was estimated by SmartMotor. From this estimate, the weight of the active part for other air gaps were calculated. The division of the total weight between rotor and stator was 25% and 75%. The final weight was calculated as proportional dependent to the axial length and the circumference of each ring.

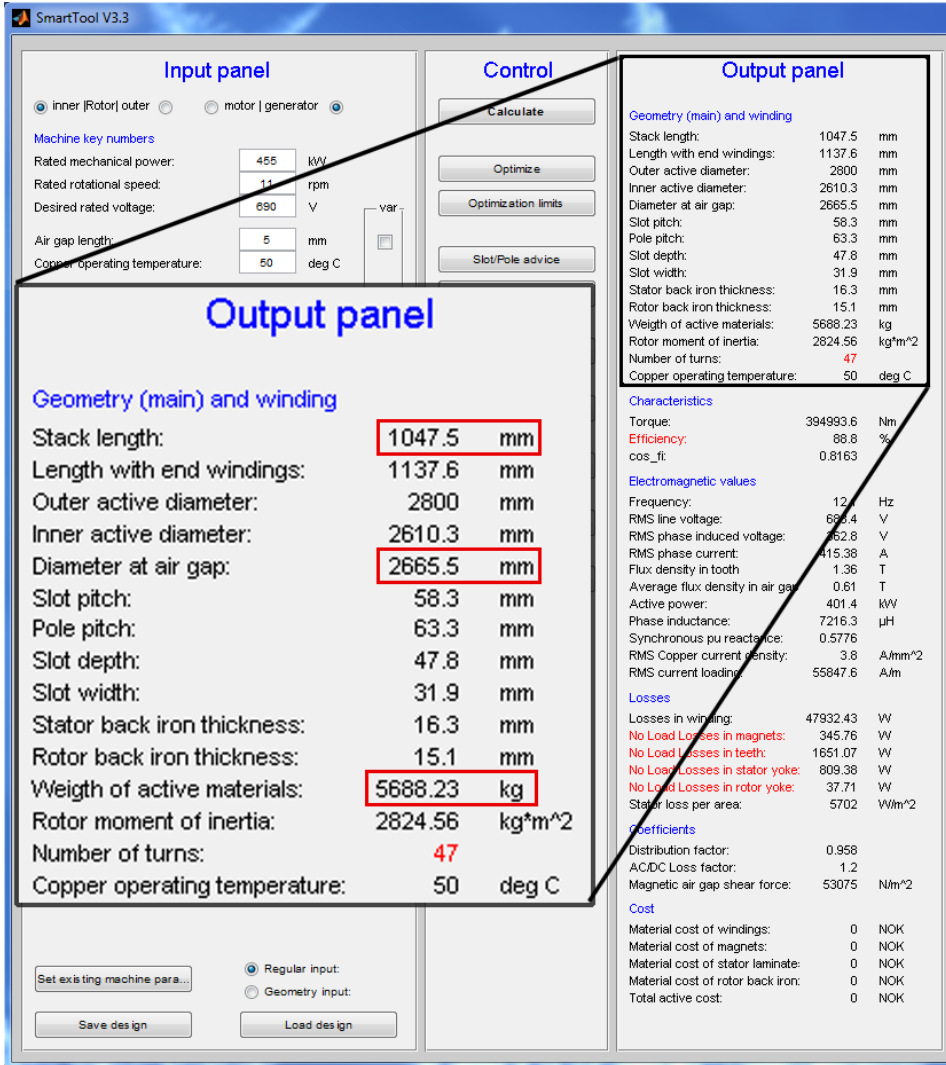


Figure 10.1: Weight calculations from electromagnetic simulations at SmartMotor

<b>Weight estimates for the stator components</b>			
<b>Component</b>	<b>Weight [kg]</b>	<b>Quantity</b>	<b>Total weight [kg]</b>
Torque plate	541	x 2	1082
Inner ring	335	x 2	670
Middle ring	689	x 2	1378
Outer ring	2429	x 1	2429
Active parts, inner ring	693	x 2	1386
Active parts, middle ring	3043	x 2	6086
Active parts, outer ring	4449	x 1	4449
<b>Total stator weight</b>	<b>17432 kg</b>		
<b>Weight estimates for the rotor components</b>			
<b>Component</b>	<b>Weight [kg]</b>	<b>Quantity</b>	<b>Total weight [kg]</b>
Torque plate	544	x 1	544
Inner ring	533	x 2	1066
Outer ring	957	x 2	1914
Active parts, inner ring	655	x 2	1310
Active parts, outer ring	1245	x 2	2490
Stiffening plates and ring	97	x 1	97
Rails, inner ring	4.1	x 44	180
Rails, outer ring	4.9	x 66	323
<b>Total rotor weight</b>	<b>7924 kg</b>		
<b>Total rotor and stator weight</b>	<b>25356 kg ≈25.4 tons</b>		
<b>Weight of other components</b>			
<b>Component</b>	<b>Weight</b>	<b>Quantity</b>	<b>Total weight [kg]</b>
Axle	2398	1	2398
Bearings	?	2	?
Electronics	?	?	?

**Table 10.1:** Weight estimates for the generator parts



# 11 Appendix F - Power output calculations

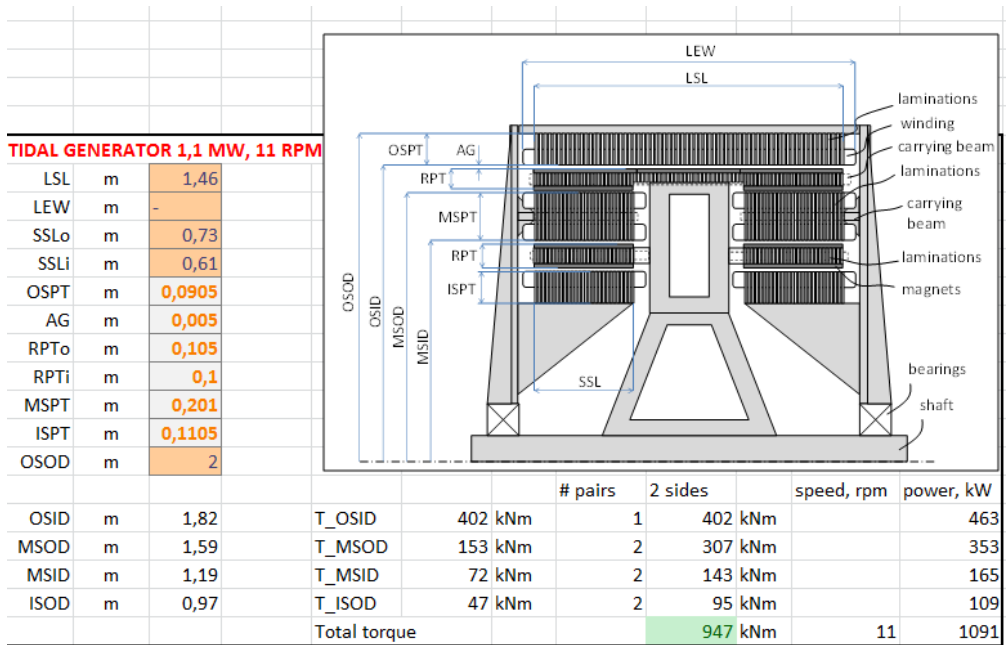


Figure 11.1: Power output calculations. Screenshot from Excel



# Bibliography

- [1] "Smartmotor as." [Online]. Available: <http://www.smartmotor.no>
- [2] "Atlantis resources corporation." [Online]. Available: <http://www.atlantisresourcescorporation.com/>
- [3] "Ces edupack 2011." [Online]. Available: <http://www.grantadesign.com/education/software.htm>
- [4] "Iec 61400-4/-1:2007 - iec international standards regarding wind turbines."
- [5] "Standard for certification no. 2.7-3 - portable offshore units - may 2011."
- [6] "En 13445-6/-3:2009 : Unfired pressure vessels."
- [7] "Sway." [Online]. Available: <http://www.sway.no>

